RESEARCH PAPER

The ABI5-dependent down-regulation of mitochondrial ATP synthase OSCP subunit facilitates apple necrotic mosaic virus infection

Chengyong He[1,2], Fei Xing[3], Jiahui Liang[4], Zhixiang Zhang[2], Binhui Zhan[2], Nuredin Habili[5], Hongqing Wang[1,*] and Shifang Li[2,*]

[1] Department of Fruit Science, College of Horticulture, China Agricultural University, Beijing 100193, China
[2] State Key Laboratory of Biology of Plant Diseases and Insect Pests, Institute of Plant Protection, Chinese Academy of Agricultural Sciences, Beijing 100193, China
[3] National Citrus Engineering Research Center, Citrus Research Institute, Southwest University, Chongqing 400712, China
[4] Institute of Grassland, Flowers and Ecology, Beijing Academy of Agriculture and Forestry Sciences, Beijing 100097, China
[5] The Australian Wine Research Institute Waite Precinct, University of Adelaide, Adelaide 5000, Australia

* Correspondence: lishifang@caas.cn or wanghq@cau.edu.cn

Abstract

Apple necrotic mosaic virus (ApNMV) is associated with apple mosaic disease in China. However, the mechanisms of ApNMV infection, as well as host defence against the virus, are still poorly understood. Mitochondrial ATP synthase plays a fundamental role in the regulation of plant growth and development. However, mitochondrial ATP synthase function in response to virus infection remains to be defined. In the present study, a yeast two-hybrid (Y2H) screening revealed that the apple mitochondrial ATP synthase oligomycin sensitivity-conferring protein (OSCP) subunit (MdATPO) interacts with ApNMV coat protein (CP). It was further verified that overexpression of *MdATPO* in *Nicotiana benthamiana* inhibited viral accumulation. In contrast, silencing of *NbATPO* facilitated viral accumulation, indicating that ATPO plays a defensive role during ApNMV infection. Further investigation demonstrated that ApNMV infection accelerated abscisic acid (ABA) accumulation, and ABA negatively regulated *ATPO* transcription, which was related to the ability of ABA insensitive 5 (ABI5) to bind to the ABA-responsive elements (ABREs) of the *ATPO* promoter. Taken together, our results indicated that transcription factor ABI5 negatively regulated *ATPO* transcription by directly binding to its promoter, leading to the susceptibility of apple and *N. benthamiana* to ApNMV infection. The current study facilitates a comprehensive understanding of the intricate responses of the host to ApNMV infection.

Keywords: ABA, ABI5, apple necrotic mosaic virus, ATPO, mitochondrial ATP synthase, OSCP.

Introduction

Apple (*Malus domestica*) is one of the most economically important fruit crops around the world, however its yield and economic benefits are restricted by biotic and abiotic stress. Apple mosaic disease (AMD) is one of the most serious threats to apple production, and it is widespread in the world's major apple-producing countries (Noda *et al.*, 2017; Xing *et al.*, 2018). Recent studies revealed that apple necrotic mosaic virus (ApNMV) is significantly associated with AMD in China (Noda *et al.*, 2017; Xing *et al.*, 2018; Shi *et al.*, 2020; Zhang *et al.*, 2022). ApNMV belongs to the genus *Ilarvirus*; nevertheless, research on *Ilarvirus* has been confined to analysis of its molecular characteristics (Aparicio *et al.*, 2003; Vlot *et al.*, 2003; Pallas *et al.*, 2013) and transmission studies (Amari *et al.*, 2007). Our recent study indicated that the coat protein (CP) of *Ilarvirus* plays a critical role in viral long-distance movement (He *et al.*, 2023). However, the molecular mechanisms underlying viral pathogenicity of the *Ilarviruses* are still poorly understood.

Mitochondria are critical double-membrane bound organelles known as 'powerhouses' that provide energy to eukaryotes for their cellular demands in the form of adenosine triphosphate (ATP) created by the respiratory chain complex (Logan, 2006; Roger *et al.*, 2017; Møller *et al.*, 2021). In addition to generating the majority of the energy or ATP needed by the cell, plant mitochondria contribute to biotic stress responses (S. Huang *et al.*, 2016). *Pseudomonas syringae* pv. *phaseolicola* infection led to a strong induction of alternative oxidases (AOX) in tobacco, which was a potentially critical regulator of a mitochondrial O_2^--based signalling pathway that ultimately affects the response of plants to bacterial infection (Cvetkovska and Vanlerberghe, 2012, 2013). The overexpression of an outer membrane protein, AAA ATPase *AtOM66* causes increased sensitivity to programmed cell death (PCD), resulting in resistance to the biotrophic pathogen *Pseudomonas syringae*, while it induced hypersensitivity to the necrotrophic pathogen *Botrytis cinerea* in *A. thaliana* (Zhang *et al.*, 2014). On the other hand, the effector *Magnaporthe oryzae* cell death–inducing protein 4 (MoCDIP4) perturbs mitochondrial dynamics and inhibits mitochondria-mediated immunity (G. Xu *et al.*, 2020). However, relatively little research has been conducted to establish whether mitochondria have a critical role in plant responses to plant viruses.

Mitochondrial ATP synthase (also known as complex V or F1F0-ATP synthase) is the enzyme responsible for oxidative phosphorylation and the synthesis of ATP from ADP. It is made up of a membrane-spanning F0 and a soluble F1 component (Müller and Grüber, 2003): the F1 domain is composed of an α3β3 hexamer, and one copy of each subunit γ, δ, and ε; and the F0 domain is composed of a ring of c subunits and one copy of each subunit a, b, d, F6, and an oligomycin sensitivity-conferring protein (OSCP). The OSCP subunit (ATPO) was assumed to form a rigid link between the peripheral stalk and the F1 head. The role of mitochondrial ATP synthase subunits during abiotic stress responses has been studied. ATP6 expression was induced during salt excess, drought, and low temperatures in Arabidopsis, and its overexpression induced a significant increase in resistance against the aforementioned abiotic stresses (Zhang *et al.*, 2008). Oxidative burst negatively impacts mitochondrial ATP synthase and degradation of subunits α, β, and d in Arabidopsis (Sweetlove *et al.*, 2002). Wheat F1F0-ATPase activities were both induced during aluminium stress, and protein expression of the α- and β-subunits all increased in response to Al (Hamilton *et al.*, 2001). However, the identity of mitochondrial ATP synthase subunits in response to biotic stress remains to be determined.

Basic region/leucine zipper motif (bZIP) transcription factor (TF), characterized by a basic leucine zipper domain, is an important TF family that regulates a variety of plant developmental processes (Strathmann *et al.*, 2001; Smykowski *et al.*, 2010; Dröge-Laser and Weiste, 2018; Kaur *et al.*, 2021) and contribute to plant abiotic responses (Kang *et al.*, 2002; Assunção *et al.*, 2010; Yue *et al.*, 2019). In addition, members of bZIPs also contribute to plant response to viruses. Pepper *PPI1* was induced during an incompatible interaction following inoculation with pepper mild mottle virus (PMMV; Lee *et al.*, 2002). Similarly, *Petunia hybrida* ocs element binding factor 1 (*PhOBF1*) was up-regulated by tobacco rattle virus (TRV), and *PhOBF1* silencing resulted in the down-regulation of RNA silencing-related genes, while the *PhOBF1*-overexpressing lines exhibited enhanced resistance to TRV and tobacco mosaic virus (TMV; Sun *et al.*, 2017).

Abscisic acid-insensitive 5 (ABI5), a member of the plant bZIP family, is the best-studied critical molecule in the abscisic acid (ABA) signalling pathway (Yu *et al.*, 2015). It has been demonstrated that ABI5 contributes to seed dormancy in *Sorghum bicolor* (Cantoro *et al.*, 2013), germination in *Arabidopsis thaliana* (Kanai *et al.*, 2010; Jin *et al.*, 2018), maturation and longevity in *Medicago truncatula* (Zinsmeister *et al.*, 2016), as well as flowering time (Xiong *et al.*, 2019) and plant growth in *Arabidopsis thaliana* (Yu *et al.*, 2015). Recently, NbABI5 was found to bind to the ABA response elements in the *NbFD1* promoter, resulting in *NbFD1* down-regulation, which facilitates rice stripe virus (RSV) infection (Cui *et al.*, 2021). However, it remains to be determined whether ABI5 is also involved in any other plant virus infections, and if so, what role it plays.

The aim of the present study was to identify and characterize the role of the mitochondrial ATP synthase subunit OSCP (ATPO) in plant immunity. Here we report that both *MdATPO* and *NbATPO* are down-regulated by ApNMV infection, and *NbATPO*-silenced *N. benthamiana* plants promoted ApNMV accumulation, while the ectopic expression

of *MdATPO* in *N. benthamiana* displayed increased resistance to infection with ApNMV. Further experiments showed that ABI5 binds directly to the ABRE (ABA–responsive elements) on the *ATPO* promoter and suppresses the expression of *ATPO*.

Materials and methods

Plant materials and growth conditions

The wild-type and transgenic *Nicotiana benthamiana* seedlings were grown in soil in a greenhouse at 25 °C under a 16 h light/8 h dark photoperiod. Tissue-cultured seedlings of *Malus domestica* 'Royal Gala' (seedling clone GL-3) (Dai *et al.*, 2013) and 'Fuji' plants were grown on Murashige and Skoog (MS) medium containing 0.3 mg l^{-1} 6-benzyl-aminopurine (6-BA) and 0.2 mg l^{-1} indoleacetic acid (IAA) in a climate-controlled chamber at 25 °C under a 16 h light (120 μmol photons m^{-2} s^{-1}) /8 h dark cycle.

Cloning and sequence analysis of MdATPO

'Fuji' leaves cDNA was used as a template to amplify the full-length coding sequence (CDS) of *MdATPO* (XM_008358516.3) using gene-specific primers (Supplementary Table S1). Multiple sequence alignments were performed using BioEdit version7.2. Complete annotated amino acid sequences of ATPO in the selected species were obtained from the National Center for Biotechnology Information (https://www.ncbi.nlm.nih.gov/). Phylogenetic analysis was performed by MEGA7.0 using the neighbor-joining method with 1000 bootstrap.

Sub-cellular localization

The pCAMBIA1300-GFP vector (Liang *et al.*, 2022) driven by the 35S promoter was used for the sub-cellular localization assay. *MdATPO* CDS without the stop codon was cloned into pCAMBIA1300-GFP to generate 35S-MdATPO-GFP^C. The empty vector 35S-GFP was used as a control. The recombinant vector 35S-MdATPO-GFP^C and empty vector 35S-GFP were transformed into *A. tumefaciens* GV3101, and then introduced into *N. benthamiana* leaves through *A. tumefaciens*-mediated infiltration (Liang *et al.*, 2022). The GFP fluorescence was observed under a confocal laser scanning microscope (LSM980; Carl Zeiss, Germany) at 48–72 hours post-infiltration (hpi). The primers used for vector construction are listed in Supplementary Table S1.

RNA extraction and quantitative real-time PCR analysis

Total RNA was extracted from *N. benthamiana* leaves by TRIzol reagent (ET101-01-V2, TransGen, Beijing, China) or from apple leaves using RNAprep Pure Plant Plus Kit (TianGen, China) following the manufacturer's instructions. The concentration and quality of total RNA were evaluated using a Nano-300 spectrophotometer (Allsheng, China) and 1.5% agarose gel electrophoresis. First-strand cDNAs were synthesized from 1 μg of total RNA using the HiScript® III RT SuperMix kit (R323-01, Vazyme, Nanjing, China). Quantitative real-time PCR (RT–qPCR) reactions with a 20 μl volume containing 0.5 μl of cDNA as the template were performed using Taq Pro Universal SYBR qPCR Master Mix (Q712-02, Vazyme, Nanjing, China) on a MyGo Pro real-time PCR instrument (IT-IS Life Science Ltd, Republic of Ireland). The mRNA level of *NbPP2A* (MF996339) or *MdEF1α* (MDP0000294265) was determined and used to normalize transcript amounts of test genes in *N. benthamiana* and apple, respectively. The second control genes

NbF-BOX (Niben.v0.3.Ctg24993647; Liu *et al.*, 2012) and *MdACTB* (XM008393049) were used to validate the stable expression of the reference genes in all the analysed samples in *N. benthamiana* and apple, respectively. The relative expression levels were calculated using the 2$^{-\Delta\Delta CT}$ method (Livak and Schmittgen, 2001). All experiments were replicated at least three times. The primers used for RT–qPCR analysis are listed in Supplementary Table S1.

Agrobacterium-mediated transformation

For ApNMV infection of *N. benthamiana* plants, the three genomic RNAs of ApNMV were isolated from apple plants in China (Xing *et al.*, 2018) and independently cloned into the pCass4-Rz vector using an In-Fusion Cloning Kit (C112-02, Vazyme, Nanjing, China) and transformed into *A. tumefaciens* EHA105. In brief, the *Agrobacterium* cultures were resuspended in infiltration buffer (10 mM MES, 10 mM MgCl$_2$, 200 μM acetosyringone) to OD$_{600}$=1.0, then incubated in a dark environment for 2−4 h at 25 °C. The three components of *Agrobacterium* cell suspensions were mixed in a 1:1:1 ratio then infiltrated into *N. benthamiana* leaves using a sterile syringe, followed by gene expression analysis and ABA quantification.

Virus-induced gene silencing

The tobacco rattle virus (TRV) vectors pTRV1 and pTRV2 (Liu *et al.*, 2002) were used for silencing endogenous genes in *N. benthamiana* plants. Given the high homology of gene sequences in *N. tabacum* and *N. benthamiana*, the sequences of *NtATPO* (XM009613739) and *NtABI5* (XM016603577) were used for designing gene silencing primers. For silencing *NbATPO* and *NbABI5*, 304 bp and 298 bp fragments, respectively, targeting unique regions, were amplified (Supplementary Table S2). The fragments were then cloned into *Eco*RI/*Bam*HI sites of the pTRV2 vector using a ClonExpress II One Step Cloning Kit (Vazyme, Nanjing, China). pTRV1, pTRV2, and its derivatives were transformed into *A. tumefaciens* strain GV3101. A combination of *Agrobacterium* colonies harbouring pTRV1 and pTRV2:NbATPO or pTRV1 and pTRV2:NbABI5 were infiltrated into *N. benthamiana* plants using a sterile syringe. *N. benthamiana* plants infiltrated with a mixture of colonies harbouring pTRV1 and pTRV2:NbPDS were used as positive controls; pTRV1 and pTRV2 co-infiltrated plants were used as negative controls. The PCR primers used for vector construction are listed in Supplementary Table S1.

Northern blot assays

The northern blot assays were performed as described previously (He *et al.*, 2023). In brief, 2 μg of total RNA from ApNMV-infiltrated *N. benthamiana* samples were separated on a 1.5% agarose gel (denaturation with 1.1% formaldehyde), and then transferred onto a Hybond-N$^+$ membrane (GE Healthcare, UK) by a vacuum transfer system. The membranes were hybridized using ApNMV probe, which was synthesized from the conserved regions at the 3′ end of genomic RNA with a DIG RNA Labeling Kit (Roche, Shanghai, China). The primers used for probe synthesis are listed in Supplementary Table S1.

Yeast two-hybrid assay

The cDNA library was constructed by the Oebiotech Company using apple leaves with ApNMV infection. The CDS of *MdATPO* was amplified and cloned into the *Eco*RI/*Bam*HI sites of the pGADT7 vector to generate AD-MdATPO. The CDS of ApNMV CP was cloned into *Eco*RI/*Bam*HI sites of the pGBKT7 vector to generate the BD-CP vector. The resulting bait and prey constructs were co-transformed into yeast strain Y2H Gold (Clontech), and cultured on SD-Leu/-Trp

medium for 2–3 d, and the co-transformants were transferred onto SD-Leu/-Trp/-His/-Ade medium to test the interactions between bait and prey proteins. The PCR primers used for vector construction are listed in Supplementary Table S1.

Bimolecular fluorescence complementation assay

The CDS of *MdATPO* and ApNMV coat protein (CP) were cloned into pUC-SPYCE and pUC-SPYNE, respectively, to generate the cYFP-MdATPO and nYFP-CP vectors. The resulting constructs were transferred into *A. tumefaciens* strain GV3101 and cultivated at 28 °C for 24 h. The cultures were resuspended in infiltration buffer (10 mM MES, 10 mM MgCl$_2$, 200 μM acetosyringone) with OD600=1.0. *Agrobacterium* strain GV3101 with cYFP-MdATPO and nYFP-CP were mixed (1:1 ratio) and then infiltrated into *N. benthamiana* leaves. Yellow fluorescent protein (YFP) signals were observed under a confocal laser scanning microscope (LSM980; Carl Zeiss, Germany) at 2–3 days post-infiltration (dpi). The primers used for vector construction are listed in Supplementary Table S1.

Yeast one-hybrid assay

For Y1H assay, the CDS of *MdABI5* (MD12G1034900) was cloned into pGADT7 to generate pGADT7-MdABI5. Then the fragment containing three tandem copies of the ABRE-box (ACGTG) or its mutant (mABRE-box; ATTTG) were synthesized and cloned into the pAbAi vector to generate pAbAi-3×ABRE or pAbAi-3×mABRE. The recombinant vectors pGADT7-MdABI5 and pAbAi-3×ABRE (or with pAbAi-3×mABRE) were co-transferred into yeast strain Y1H Gold and cultured on SD/−Leu medium, and then successful transformants were transferred to screening plates SD/-Leu with 200 ng ml^{-1} AbA at 30 °C for 3 d. The primers are listed in Supplementary Table S1.

Quantification of ABA

A total of 1–1.5 g of leaves from ApNMV or mock-inoculated *N. benthamiana* plants were collected, and ABA was extracted using a mixture of isopropanol/water/hydrochloric acid. The extracts were dissolved in methyl alcohol and purified through a 0.22 μm filter membrane, then analysed using a HPLC-MS/MS detection system (HPLC, Agilent1290, https://www.agilent.com; MS/MS, Applied Biosystems 6500 Quadrupole Trap, https://sciex.com.cn/). This work was done by Nanjing Convinced-test Technology Co, Ltd (http://www.convinced-test.com/plant-hormone.html).

Exogenous abscisic acid treatment

Abscisic acid (Aladdin, Shanghai, China) was dissolved in 100% ethanol to a stock concentration of 100 mM and diluted with double-distilled H$_2$O to a final concentration of 100 μM when utilised. ABA solutions was sprayed onto fully expanded leaves until they were entirely moist. H$_2$O was used to spray control plants.

Co-immunoprecipitation assay

The CDS of ApNMV CP was cloned into the pCAMBIA1300-GFP vector to generate GFP-ApNMV CP. Likewise, the CDS of *MdATPO* was cloned into the pGD-3×Flag vector to generate the 3×Flag-MdATPO. *A. tumefaciens* harbouring 3×Flag-MdATPO and GFP-ApNMV CP or empty GFP constructs were co-infiltrated into *N. benthamiana* leaves. Total proteins were extracted from the agroinfiltrated *N. benthamiana* leaves at 3 dpi with IP buffer [0.15 M NaCl, 0.05 M Tris-HCl, pH 7.5, 1 mM EDTA, 0.1% (v/v) Triton X-100, 10% (v/v) glycerol, 1×protease inhibitor cocktail (SL1086, Coolaber) and 1 mM phenylmethylsulfonyl fluoride (PMSF,

PP2701, Aidlab)], followed by centrifugation of samples at 10 000 × *g* for 5 min. The supernatant was incubated with 20 μl of Anti-Flag Magnetic Beads (P2115, Beyotime, Shanghai, China) on a rotator at 4 °C for 2 h. The beads were separated using a magnetic rack and washed five times using 1×TBS buffer, and then adsorbed proteins were eluted from the beads with 3×Flag peptide (P9801, Beyotime) and analysed by immunoblotting using anti-Flag and anti-GFP antibodies. The primers used for vector construction are listed in Supplementary Table S1.

Transcriptional activity assay

Assays of transcriptional activation activity were performed using the yeast system. *MdABI5* CDS was cloned into PGBKT7 (Oebiotech, Shanghai, China), resulting in BD-MdABI5 containing the GAL4 DNA-binding domain. GAL4 and PGBKT7 were used as the positive and negative controls, respectively. The resulting constructs were introduced into yeast strain AH109 and cultured on SD/−Trp medium at 30 °C for 3 d, and then the transformants were transferred to screening plates with SD/-Trp-His. β-galactosidase activity was measured by LacZ-filter lift assays, according to the method described previously (Liang *et al.*, 2022). The transcriptional activity in *N. benthamiana* leaves was further examined using a transient luciferase (LUC) expression system, as described by Liang *et al.* (2022). *MdABI5* CDS was cloned into the PEAQ vector, resulting in PEAQ-MdABI5 as the effector vector, and then co-infiltrated with pGreenII0800-LUC driven by the 5×*USA GAL* promoter into *N. benthamiana* leaves. The LUC fluorescence of the agroinfiltrated leaves was measured after 48 h using an automatic chemiluminescence image analysis system (Tanon 5200, Tanon, Shanghai, China). LUC and REN activities were determined using the dual-luciferase reporter assay reagents (11402ES60, Yeasen, Shanghai, China) on a Microplate Reader (FlexStation 3, Molecular Devices, USA); REN was used as an internal reference. Primers used for vector construction are listed in Supplementary Table S1.

GUS activity assay

The 1860 bp fragment before the start codon of *MdATPO* was cloned into the pCAMBIA1391 vector to generate a Pro*MdATPO*-GUS reporter vector. The CDS of *MdABI5* was cloned into the pCAMBIA1300-GFP vector driven by the 35S promoter to generate 35S-MdABI5-eGFP effector construct. The empty vector was used as a negative control. The recombinant vectors were co-transferred into leaves of *N. benthamiana* or tissue-cultured apple seedlings by vacuum infiltration (65 kPa, 3 min). Infiltrated leaves were harvest at 48 h post-infection and incubated with a GUS staining kit (SL7160, Coolaber, Beijing, China) overnight at 37 °C, and then decolorized using 100% ethanol and photographed. To quantify the relative expression of *GUS* gene, infiltrated leaves were collected and used for RT–qPCR. Primers used for vector construction and RT–qPCR are listed in Supplementary Table S1.

Dual-luciferase reporter assay

The CDS of *MdABI5* was cloned into the pGreenII 62-SK to generate the effector vector, and the 1860 bp promoter of *MdATPO* was cloned into pGreenII 0800-LUC to generate the reporter vector. The empty vector was used as the negative control. The recombinant vectors were transformed into *A. tumefaciens* strain GV3101 harbouring the pSoup helper plasmid, and cultivated overnight at 28 °C in Luria Bertani (LB) medium with kanamycin (50 μg ml^{-1}) and rifampicin (25 μg ml^{-1}). *A. tumefaciens* was collected and adjusted to OD$_{600}$=1.0 using infiltration buffer (10 mM MES, 10 mM MgCl$_2$, 200 μM acetosyringone). The *Agrobacterium tumefaciens* cultures with empty and effector constructs were mixed with the reporter vector in a 4:1 ratio (v/v), respectively, and then infiltrated into *N. benthamiana* leaves using a needleless syringe. The LUC fluorescence of the agroinfiltrated leaves was measured after 48 h using

an automatic chemiluminescence image analysis system (Tanon 5200, Tanon, Shanghai, China). LUC and REN activities were determined, and the LUC/REN ratio for representing the relative promoter activity was calculated; REN was used as an internal reference. All primers are listed in Supplementary Table S1.

Statistical analysis

Means of at least three biological replicates were calculated with GraphPad Prism v.8.00. Values are presented as means ±SD. Statistical significance was determined using Student's *t*-test, *$P<0.05$; **$P<0.01$.

Results

Expression pattern of MdATPO

In ilarvirus, the CP is necessary for initiation of infection and cell-to-cell movement (Aparicio *et al.*, 2010). Recently, we found that the CP of ilarvirus is required for viral long-distance movement (He *et al.*, 2023). As obligate intracellular organisms, plant viruses must utilize host factors for their infection process. To understand the functional mechanism of ApNMV CP during ApNMV infection, we performed a Y2H assay using ApNMV CP as a bait to screen an apple (*Malus domestica*) cDNA library and to identify the probable protein(s) that interact with the CP. MdATPO (GenBank accession no. XM_008358516.3), a known mitochondrial ATP synthase subunit OSCP, was identified as a putative CP interactor. A multiple sequence alignment based on MdATPO amino acid sequence and ATPO homologs of *Zea mays*, *Nicotiana tomentosiformis*, *Arabidopsis lyrata*, *Cucumis sativus,* and *Oryza sativa* indicated that MdATPO showed a highly conserved OSCP superfamily motif with other species (Fig. 1A). Phylogenetic analysis indicated that MdATPO was closely related to proteins from the rosaceous species, while more distantly related to orthologous proteins from other species (Fig. 1B).

To clarify the sub-cellular location of MdATPO in the plant cell, the coding sequence (CDS) of *MdATPO* was cloned into the pCAMBIA1300 vector and then the 35S-MdATPO-GFP^C construct was transformed into *Nicotiana benthamiana* (*N. benthamiana*) leaves via *Agrobacterium*-mediated infiltration. Strong GFP fluorescence was observed in the plasma membrane, cytoplasm, and nucleus (Fig. 1C). To better understand the expression pattern of *MdATPO* in apple, tissue-specific expression during different developmental stages of 'Fuji' apple was assessed by real-time quantitative reverse transcription PCR (RT–qPCR). The results showed that *MdATPO* was strongly expressed in the mature leaves, and less expression was found in stems, shoot, young leaves and fruits, with weak expression in the roots (Fig. 1D).

MdATPO interacts with ApNMV CP in vitro and in vivo

To confirm the interaction between MdATPO and ApNMV CP, Y2H assays were performed (Fig. 2). The coding sequences

of *MdATPO* and CP were inserted into pGADT7 and pGBKT7, respectively, and then co-transformed into yeast strain Y2H Gold. The yeast colonies harbouring AD-MdATPO and BD-CP grew well on the selective synthetic defined medium SD/−Trp/−Leu/−His/−Ade (QDO), while the negative control could not grow on the QDO medium, suggesting that there was an interaction between MdATPO and ApNMV CP *in vitro* (Fig. 2A).

We next used a bimolecular fluorescence complementation (BiFC) assay to verify the interaction between MdATPO and ApNMV CP. *Agrobacterium* harbouring cYFP-MdATPO and nYFP-CP constructs were co-infiltrated into *N. benthamiana* leaves. Strong yellow fluorescence signals were observed in the cytoplasm and nucleus under a confocal microscope (Fig. 2B, upper panel) at 48 hpi. However, the negative control combinations of cYFP-MdATPO with nYFP (Fig. 2B, middle panel) and nYFP-CP with cYFP (Fig. 2B, lower panel) produced no fluorescence signals. These data indicated that ApNMV CP physically interacted with MdATPO in the cytoplasm and nucleus *in vivo*.

To further confirm the above results, we performed a co-IP assay using *N. benthamiana* leaves. Accordingly, we cloned the *MdATPO* and CP coding sequences in frame with that of 3×Flag peptide and the GFP tag, respectively. We then transiently co-infiltrated 3×Flag-MdATPO and GFP-CP or GFP constructs into *N. benthamiana* leaves, followed by total protein extraction at 3 dpi and immunoprecipitation with anti-Flag magnetic beads. Immunoblot analysis revealed that 3×Flag-MdATPO co-precipitated with GFP-CP but not with control GFP (Fig. 2C). To complement the co-IP assays, we confirmed the CP-MdATPO interactions using a luciferase complementation imaging assay. Luciferase signals were observed when nLuc-CP and cLuc-MdATPO were co-infiltrated into *N. benthamiana* leaves, and no luciferase signal was detected in negative controls (Fig. 2D), suggesting that MdATPO interacts with the CP *in vivo*. Collectively, these data demonstrated that MdATPO interacts with ApNMV CP both *in vitro* and *in vivo*.

ATPO contributes to resistance to ApNMV

To investigate the potential biological functions of *ATPO* during ApNMV infection, we first examined the *MdATPO* transcript levels in ApNMV-infected apples. RT–qPCR analysis revealed that *MdATPO* mRNA levels in ApNMV-infected plants declined by roughly 61% compared with the non-infected plants (Fig. 3A). A time course analysis of *NbATPO* transcript levels during ApNMV infection revealed that, in contrast to the control plants infected with empty vector, *NbATPO* mRNA levels decreased steadily over time following inoculation (Fig. 3B). These results indicated that ApNMV infection suppressed *ATPO* transcription in both *N. benthamiana* and its natural host apple.

To investigate how *MdATPO* responds to ApNMV, *MdATPO* was ectopically expressed in *N. benthamiana* plants. Three stable
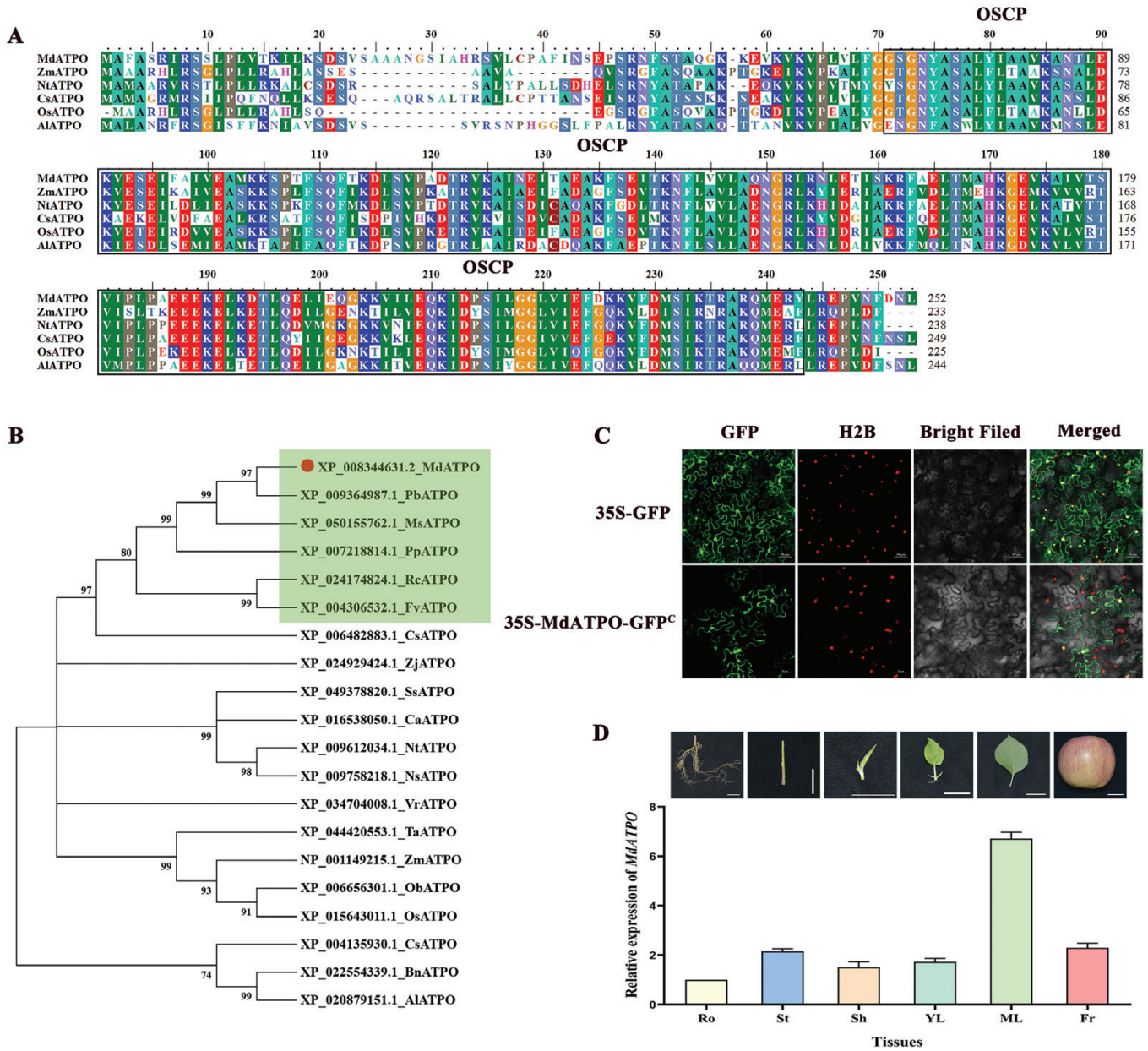
Fig. 1. Amino acid sequence alignment, phylogenetic analysis, sub-cellular localization, and expression pattern of MdATPO. (A) The amino acid sequence alignment of MdATPO with ATPO homologs in *Zea mays* (ZmATPO, NP_001149215.1), *Nicotiana tomentosiformis* (NtATPO, XP_009612034.1), *Cucumis sativus* (CsATPO, XP_004135930.1), *Oryza sativa* (OsATPO, XP_015643011.1) and *Arabidopsis lyrata* (AlATPO, XP_020879151.1). The box contains the conserved super OSCP motif with 143 aa residues. (B) Phylogenetic analysis of ATPO proteins from *N. tomentosiformis* (NtATPO), *C. sativus* (CsATPO), *Oryza sativa* (OsATPO), *Arabidopsis* (AlATPO), *Solanum stenotomum* (SsATPO), *Zea mays* (ZmATPO), *Brassica napus* (BnATPO), *Pyrus bretschneideri* (PbATPO), *Ziziphus jujuba* (ZjATPO), *Capsicum annuum* (CaATPO), *Rosa chinensis* (RcATPO), *Vitis riparia* (VrATPO), *Citrus sinensis* (CsATPO), *Fragaria vesca* (FvATPO), *Nicotiana sylvestris* (NsATPO), *Triticum aestivum* (TaATPO), *Prunus persica* (PpATPO) *and Malus sylvestris* (MsATPO)using MEGA 7.0 software. Bootstrap values from 1000 replicates are indicated. The MdATPO from this study is indicated by the red circle, ATPO homologous proteins in rosaceous species are indicated in the green rectangle. (C) Sub-cellular localization of MdATPO. *MdATPO* fused with GFP and empty GFP-containing vectors were transiently expressed in *N. benthamiana* leaves. All images were visualized by confocal microscopy at 48–72 hpi. H2B was used as nuclei localization control. Scale bar=50 μm. (D) *MdATPO* expression pattern in different organs and tissues of apple 'Fuji'; *MdATPO* expression was relative to that in roots in all samples examined. Data are means ±SDs (*n*=3). Scale bars=2 cm. Ro, root; St, stem; Sh, shoot; YL, young leaf; ML, mature leaf; Fr, fruit.

A
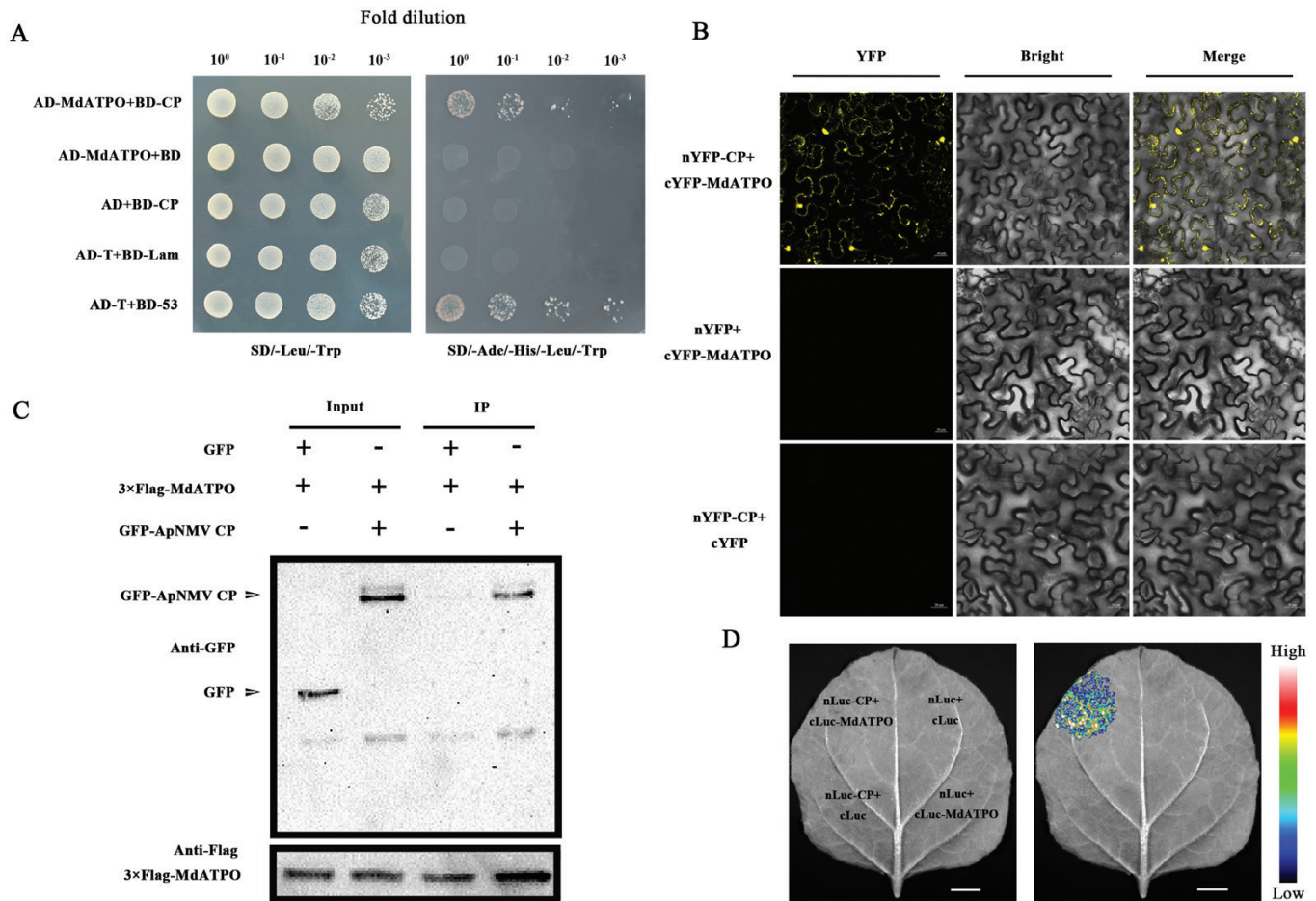
Fold dilution

Fig. 2. MdATPO interacts with ApNMV coat protein (CP) *in vitro* and *in vivo*. (A) Yeast two-hybrid (Y2H) analysis of the interaction between MdATPO and ApNMV CP. Plasmid combinations are indicated on the left and fold dilution on top of the panel. Cells of yeast strain Y2H Gold co-expressing the indicated plasmid combinations were spotted onto yeast synthetic defined (SD) medium SD/-Trp/-Leu and SD/-Trp/-Leu/-His/-Ade. The yeast cells harbouring BD+AD-MdATPO, AD+BD-CP, and AD-T+BD-lam were used as negative controls, and AD-T+BD-53 was used as positive control; the fold dilutions are indicated at the top. (B) Bimolecular fluorescence complementation (BiFC) assay demonstrated the interaction between MdATPO and ApNMV CP. Plasmid combinations were co-infiltrated into *N. benthamiana* leaves; YFP fluorescence was visualized by confocal microscopy at 2 dpi. The yellow fluorescence indicates an interaction between MdATPO and ApNMV CP. Scale bars=20 μm. (C) Coimmunoprecipitation (co-IP) assay illustrating the interaction between MdATPO and ApNMV CP. The 3×Flag-MdATPO construct was transiently co-expressed with GFP-ApNMV CP in *N. benthamiana* leaves by agroinfiltration, total protein was extracted at 3 dpi and immunoprecipitated with anti-Flag beads. Input and IP immunoprecipitation were analysed by immunoblotting with anti-GFP or anti-Flag antibodies. (D) Luciferase complementation imaging (LCI) analysis of the interaction between MdATPO and ApNMV CP. The *Agrobacterium* strain carrying the indicated constructs were infiltrated into *N. benthamiana* leaves and applied to fluorescence imaging at 2 dpi. Empty nLuc and cLuc vectors served as negative controls. Scale bars=1 cm. Colour scale on the right indicates the intensity of the captured signals.

transgenic lines were selected to determine *MdATPO* expression by RT–PCR (Supplementary Fig. S1A) and western blotting using anti–GFP antibody (Supplementary Fig. S1B). *MdATPO*-overexpressing plants did not exhibit any observable phenotypic differences from control plants (Supplementary Fig. S2). Subsequently, ApNMV was inoculated into transgenic lines by agroinfiltration at the six–leaf stage, and systemic leaves were collected at 14 dpi for immunoblot analyses. No typical symptoms were present in the empty vector and *MdATPO* transgenic *N. benthamiana* plants, while there was a significant decrease (*P*<0.01) in ApNMV accumulation in the leaves of #3.4, #3.7, and #3.9 transgenic plants compared with the

empty vector–inoculated control plants at both mRNA (Fig. 3C, D) and protein levels (Fig. 3E, F).

To further determine the role of *NbATPO* in ApNMV infection, we silenced *NbATPO* in *N. benthamiana* plants using the TRV-induced gene silencing system (VIGS) and then inoculated these plants with ApNMV after 5 d of TRV treatment. TRV:NbATPO-silenced plants showed stunted growth, and shorter leaf distances than the TRV:00–treated control plants (Supplementary Fig. S3A, F). The newly emerged leaves in the silenced plants were twisted (Supplementary Fig. S3B–D) at 14 dpi, and deformed flowers developed were aborted later (Supplementary Fig. S3E). RT–qPCR analysis revealed that
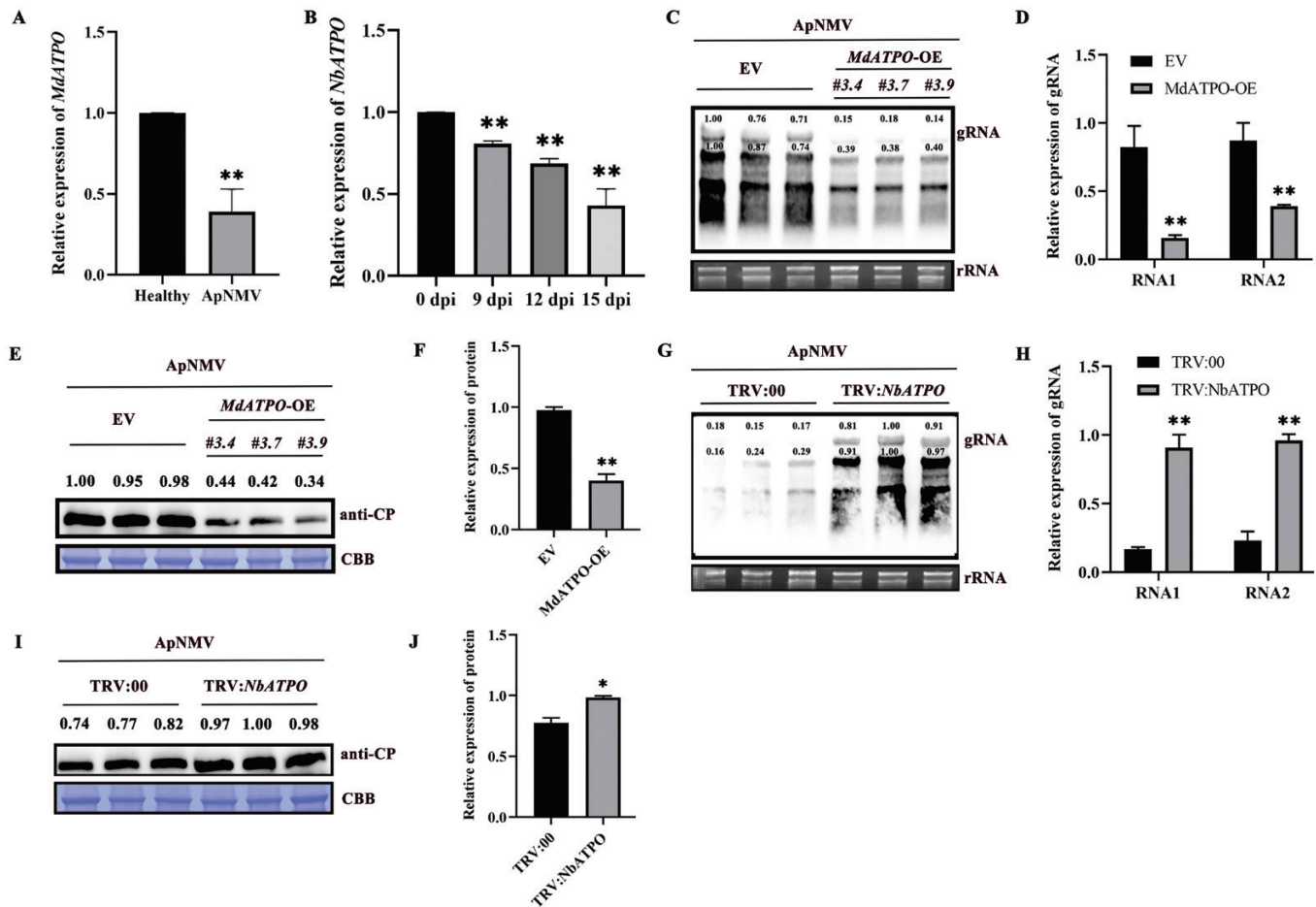
Fig. 3. ATPO positively regulates plant defence against ApNMV infection. (A) *MdATPO* is down-regulated in ApNMV-infected apple plants. Leaves from ApNMV-infected apple plants with typical symptoms were collected and subjected to RT–qPCR analysis, the expression of *MdATPO* was determined relative to that of healthy plants. Error bars indicate the SE of the mean (*n*=3). Asterisks indicate significant differences (*, *P*<0.05; **, *P*<0.01), as determined by Student's *t*-test. (B) Relative *NbATPO* transcript levels under ApNMV infection. *N. benthamiana* systemic leaves infected with empty vector (EV) or ApNMV were collected at 0, 9, 12, and 15 dpi for RT–qPCR analysis; the expression of *NbATPO* was determined relative to that of EV-treated plants. (C) Northern blot analysis of ApNMV accumulation in systemic leaves of mock-inoculated and MdATPO-overexpressed *N. benthamiana* plants at 14 dpi using a DIG-labelled specific probe that was synthesized from conserved regions at the 3' end of ApNMV genomic RNAs. ribosomal RNAs (rRNAs) stained with GelStain served as a loading control. (D) Average values were derived based on the intensity of the bands in (C), and statistical analysis was performed. (E) Western blot results showing the accumulation of ApNMV CP in inoculated *N. benthamiana* plants at 14 dpi. (F) Average values were derived based on the intensity of the bands in (E), and statistical analysis was performed. (G) Northern blot analysis of ApNMV accumulation in systemic leaves of mock-inoculated and *NbATPO*-silenced *N. benthamiana* plants at 14 dpi. (H) Statistical analysis of blot results in (G). (I) Western blot results showing the accumulation of ApNMV CP in mock-inoculated and *NbATPO*-silenced *N. benthamiana* plants at 14 dpi. (J) Statistical analysis of blot results in (I). For (E) and (I), Coomassie Brilliant Blue (CBB)-stained Rubisco large subunit served as a loading control. For (C), (E), (G) and (I), numbers above the blots indicated bands intensities. For (D), (F), (H) and (J), error bars indicate the SE of the mean (*n*=3). Asterisks indicate significant differences (*, *P*<0.05; **, *P*<0.01), as determined by Student's *t*-test. For (E) and (I), anti-CP monoclonal antibody raised against ApNMV was used. Three independent plants were used to extract total RNA and proteins. The experiments were performed independently three times and representative results are shown. The intensities of bands in northern and western blot analyses were quantified using ImageJ software to compare the virus titres.

the expression level of *NbATPO* in silenced plants was only 10% of that in the control plants (Supplementary Fig. S3G), and there were no significant differences in TRV accumulation levels (Supplementary Fig. S3H), indicating that the abnormal phenotypes of TRV: NbATPO-silenced plants were not related to the TRV titre. In addition, ApNMV in the *NbATPO* silenced plants increased significantly at both mRNA (Fig. 3G, H) and protein levels (Fig. 3I, J) in comparison with that in the TRV:00-inoculated plants.

Taken together, these results demonstrate that ApNMV in-fection down-regulates *ATPO* expression, and *ATPO* plays a defensive role during ApNMV infection.

Abscisic acid accumulates in ApNMV-infected N. benthamiana

To further investigate the possible mechanism of down-regulation of *ATPO* by ApNMV, we evaluated the probable

transcription factor binding sites in the promoters of *MdATPO* and *NbATPO* using the plant *cis*-acting regulatory element (CARE) database (http://bioinformatics.psb.ugent.be/webtools/plantcare/html/). Nine *cis*-elements involved in ABA responsiveness, nine elements involved in light responsiveness, four elements involved in methyl jasmonate (Me-JA) responsiveness, one element related to meristem expression, one element for zein metabolism regulation, one element involved in low-temperature responsiveness, and one element involved in defence and stress responsiveness were predicted from the *MdATPO* promoter (Fig. 4A; Supplementary Table S3). Likewise, 10 elements involved in light responsiveness, four elements involved in ABA responsiveness, three elements involved in gibberellin-responsive, two elements involved in Me-JA responsiveness, two elements involved in auxin responsiveness, one element related to salicylic acid responsiveness, one element for anaerobic induction, and one element involved in low-temperature responsiveness were predicted from the *NbATPO* promoter (Supplementary Fig. S4; Supplementary Table S4).

Considering the abundance of the elements involved in ABA responsiveness, we presumed that the ABA pathway responds to ApNMV infection and plays a role in regulation of *ATPO*. The results of hormone content determination showed that the concentration of ABA in ApNMV-infected *N. benthamiana* was significantly increased by about 1.6-, 2.1-, and 5-fold at 9, 12, and 15 dpi, respectively (Fig. 4B). In addition, we measured the expression level of genes related to the ABA pathway in ApNMV-infected *N. benthamiana* at 15 dpi. RT–qPCR analysis revealed that the mRNA levels of three genes involved in ABA biosynthesis, *NbABA1* (ABA deficient 1), *NbABA2* (ABA deficient 2) and *NbNCED1* (9-*cis*-epoxycarotenoid dioxygenase), were increased by 2.3- to 2.5-fold in ApNMV-infected plants compared with the control plants inoculated with empty vector (Fig. 4C–E). No clear differences in the expression of *NbABA8ox* (ABA 8'-hydroxylase), the ABA catabolism gene, were found between the control and the ApNMV-inoculated plants (Fig. 4F), indicating that ABA accumulates in *N. benthamiana* during early stages of ApNMV infection.

ABA negatively regulates NbATPO *expression and resistance to ApNMV*

To test whether ABA regulates *NbATPO* expression, we exposed *N. benthamiana* plants to 100 μM exogenous ABA, and time course changes in endogenous *NbATPO* transcription were measured using RT–qPCR. *NbATPO* expression was persistently down-regulated within 48 h post-ABA treatment, and decreased to 58% of that in control plants at 24 h after treatment (Fig. 5A), indicating that ABA negatively regulates the expression of *NbATPO*. Considering four ABA responsive *cis*-elements that are present in the promoter of *NbATPO*, we further investigated whether ABA regulates *NbATPO* promoter activity. The promoter sequence of *NbATPO* was

cloned into the pGreenII 0800-Luc vector and a dual-luciferase assay was performed. It was found that the promoter activity of *NbATPO* was suppressed by ABA (Fig. 5B). Together, these results demonstrated that ABA negatively regulates the expression of *NbATPO* by suppressing its promoter activity.

To further investigate the role of ABA in ApNMV infection, the *N. benthamiana* plants were sprayed with 100 μM exogenous ABA and agroinfiltration with ApNMV at 24 h after treatment with ABA. The inoculated leaves were harvested at 3 dpi, and total RNA was extracted and subjected to northern blot assay to evaluate the accumulation of ApNMV genomic RNA in *N. benthamiana* plants. Simultaneously, total protein was extracted from the inoculated leaves and western blot assay was performed to evaluate the expression level of ApNMV CP. Compared with that in mock-treated control plants, ABA-treated plants were significantly more susceptible ($P<0.05$) to ApNMV, which showed increased expression of viral mRNA (Fig. 5C, D) and protein (Fig. 5E, F). Collectively, these results demonstrated that ABA enhanced the accumulation of ApNMV in *N. benthamiana* plants.

ABI5 negatively regulates ATPO *expression*

The potential transcription factors in the ABA pathway that were involved in the regulation of *MdATPO* were predicted by PlantRegMap (http://plantregmap.gao-lab.org/binding_site_prediction.php). *MdABI5*, a member of the bZIP family, was predicted to bind to the ABRE element in the *MdATPO* promoter. To examine the transactivation ability of MdABI5, the full-length coding sequence of *MdABI5* was fused to the GAL4 DNA-binding domain in the pGBKT7 vector. The transformed yeast cells expressing GAL4 (positive control) and VP16, a recognized transactivation domain (Y. Xu *et al.*, 2020) grew well on SD/-Trp-His, whereas yeast cells transformed with BD (negative control) or BD-MdABI5 could not grow normally (Fig. 6A), indicating that MdABI5 lacks transactivation ability *in vitro*. To determine whether MdABI5 has transcriptional repression activity, a β-galactosidase activity assay was performed. We found that that MdABI5 blocked the transactivation function of VP16 (Fig. 6B). We then performed a dual-luciferase transactivation assay, and when compared to the control harbouring PEAQ alone, *N. benthamiana* leaves expressing the PEAQ-MdABI5 construct showed significantly lower ($P<0.01$) relative luciferase activity (Fig. 6C, D). Taken together, these results indicate that MdABI5 is a transcriptional repressor.

Next, we measured *NbABI5* expression during ABA treatment and ApNMV infection. We found that 100 μM exogenous ABA treatment increased *NbABI5* expression 6 h post-ABA treatment, and reached a maximum induction of 27.6-fold at 24 hpi compared with control plants; however, at 72 hpi, the expression level decreased rapidly (Fig. 6E). Likewise, *NbABI5* expression was strongly induced in *N. benthamiana* plants during ApNMV infection (Fig. 6F).
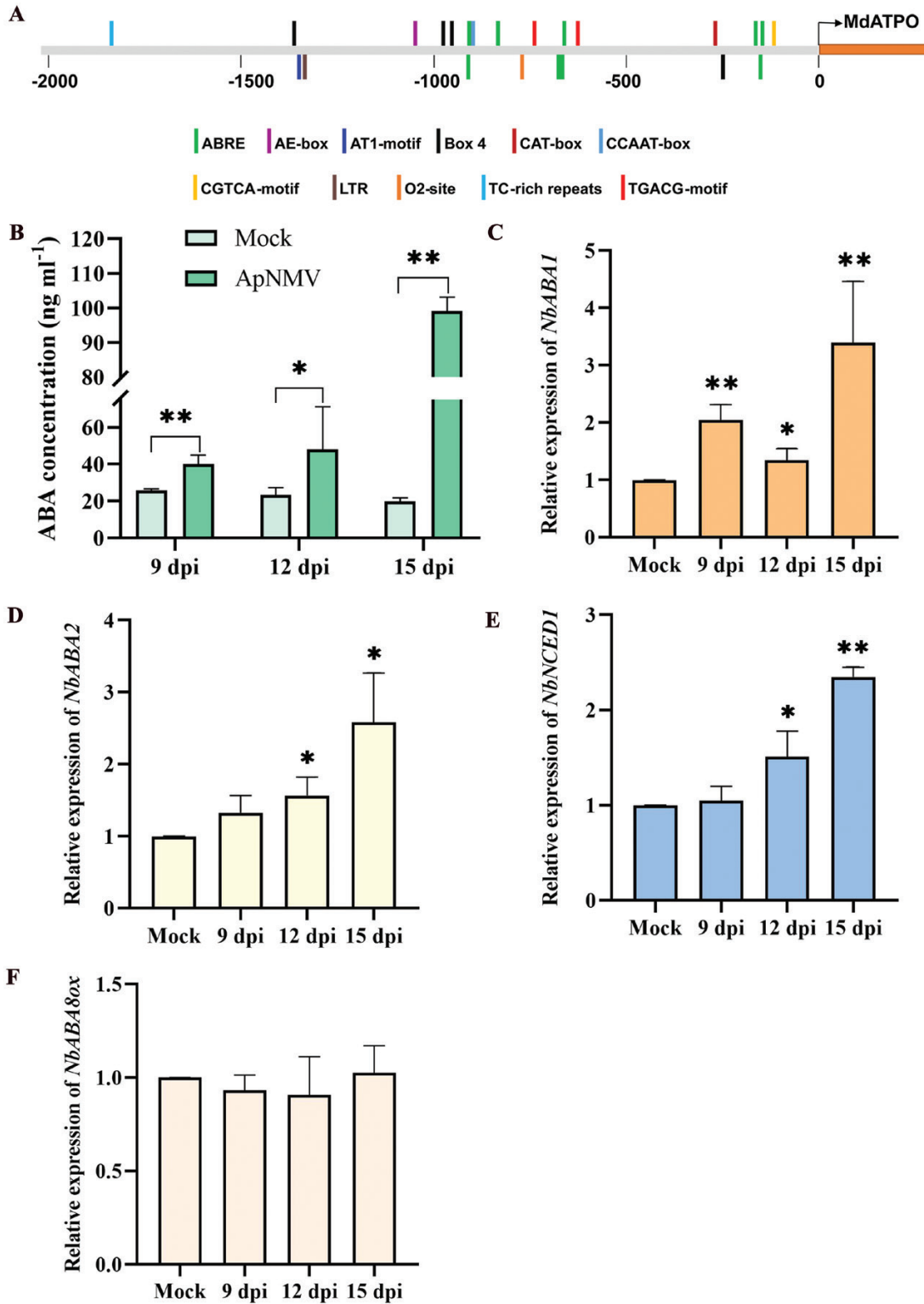
Fig. 4. Abscisic acid (ABA) accumulates in ApNMV-infected *Nicotiana benthamiana* plants. (A) The predicted *cis*-acting regulatory elements in the promoter sequences of *MdATPO*. (B) ABA concentrations in mock and ApNMV-infected *N. benthamiana* plants measured by liquid chromatography–tandem mass spectrometry at 9-, 12- and 15 dpi. (C-E) Quantitative real-time PCR (RT–qPCR) analysis revealed the transcript levels of three ABA biosynthesis genes (C) *NbABA1*, (D) *NbABA2*, and (E) *NbNCED1* in ApNMV-infected plants compared with the control plants inoculated with empty vector at 9, 12, and 15 dpi. (F) RT–qPCR showing the transcript levels of ABA catabolism gene *NbABA8ox* in mock and ApNMV-infected plants. Error bars indicate the SE of the mean (*n*=3). Asterisks indicate significant differences (*, *P*<0.05; **, *P*<0.01), as determined by two-sample unequal variance directional *t*-test. The expression of all genes was determined relative to that of mock-treated plants, respectively.
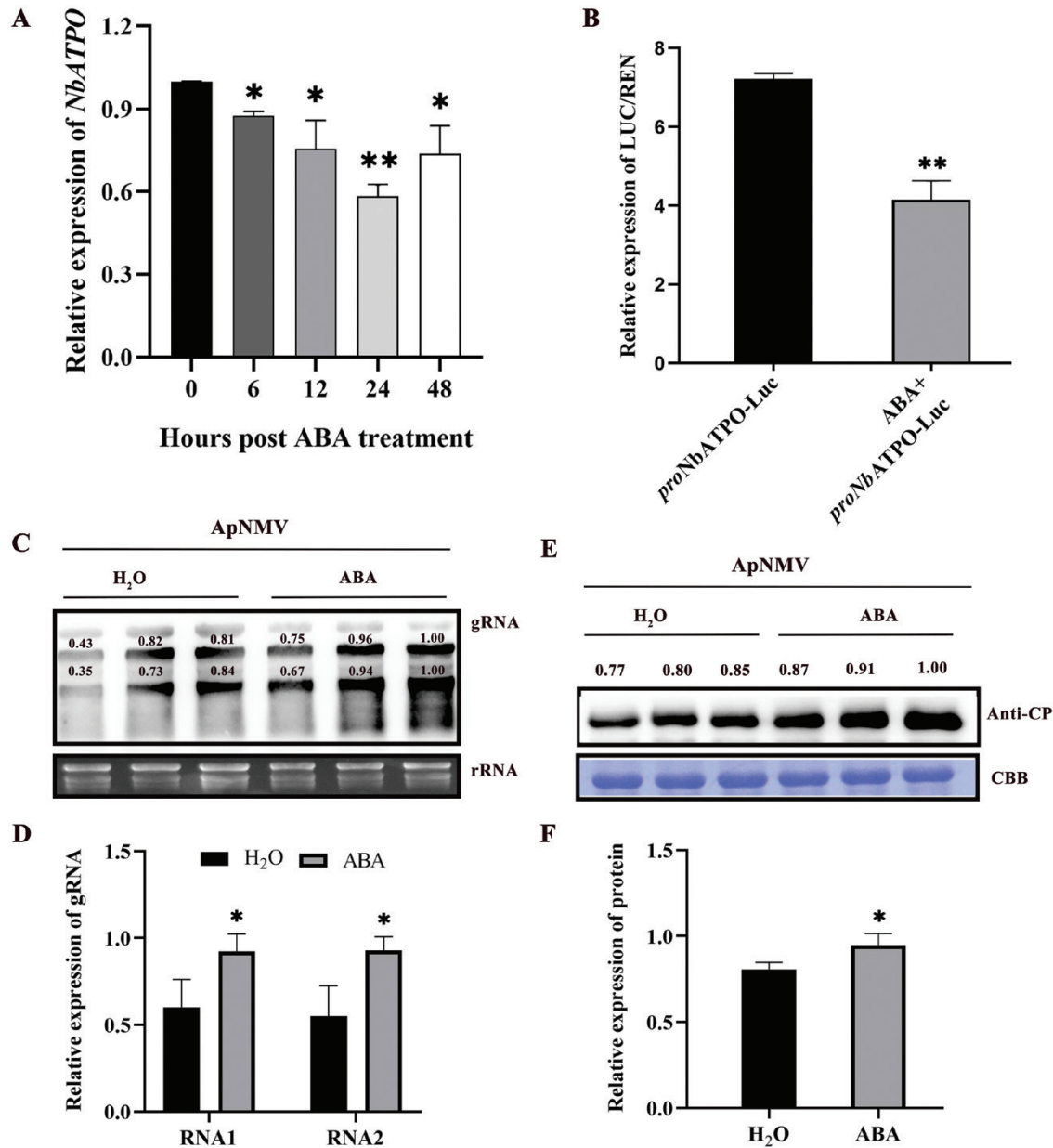
Fig. 5. ABA negatively regulates *NbATPO* expression and resistance to ApNMV. (A) Time course analysis of the transcript levels of *NbATPO* in 100 µM ABA-treated plants at 0, 6, 12, 24 and 48 h by RT–qPCR. The expression of *NbATPO* was determined relative to that of mock-treated plants. Error bars indicate the standard error (SE) of the mean (*n*=3). Asterisks indicate significant differences (*, $P<0.05$; **, $P<0.01$), as determined by two-sample unequal variance directional *t*-test. (B) Dual luciferase assay indicating the effect of ABA on *NbATPO* promoter activity. The ratio of LUC/REN of the empty vector pGreenII 0800-LUC co-transformed with *Pro*NbATPO-LUC vector was used as a calibrator. (C) Northern blot analysis of ApNMV genomic RNA accumulation in inoculated leaves of H_2O and ABA-treated *N. benthamiana* plants at 3 dpi. *N. benthamiana* leaves were sprayed with 100 µM ABA or H_2O 24 h before ApNMV inoculation, three independent samples were collected from the inoculated leaves at 3 dpi; ribosomal RNAs (rRNAs) stained with GelStain served as a loading control. (D) Statistical analysis of blot results in (C). (E) Western blot results showing the accumulation of ApNMV coat protein (CP) in inoculated leaves of H_2O and ABA-treated *N. benthamiana* plants at 3 dpi. (F) Statistical analysis of blot results in (E). Coomassie Brilliant Blue (CBB)-stained Rubisco large subunit served as a loading control. The experiments were performed independently three times and representative results are shown. The intensities of bands in western blot analyses were quantified using ImageJ software to compare the virus titre. For (C) and (E), numbers above the blots indicated bands intensities. For (D) and (F), error bars indicate the SE of the mean (*n*=3). Asterisks indicate significant differences (*, $P<0.05$; **, $P<0.01$) as determined by Student's *t*-test.

To test whether ABI5 regulates *ATPO* expression, we transiently overexpressed *NbABI5* in *N. benthamiana* plants using PVX-based vectors as described previously (Liu *et al.*, 2021), and then examined the expression of *NbATPO*. RT–qPCR analysis revealed that *NbABI5* expression increased ($P<0.01$) about 3-fold in *NbABI5*-overexpressed plants compared with
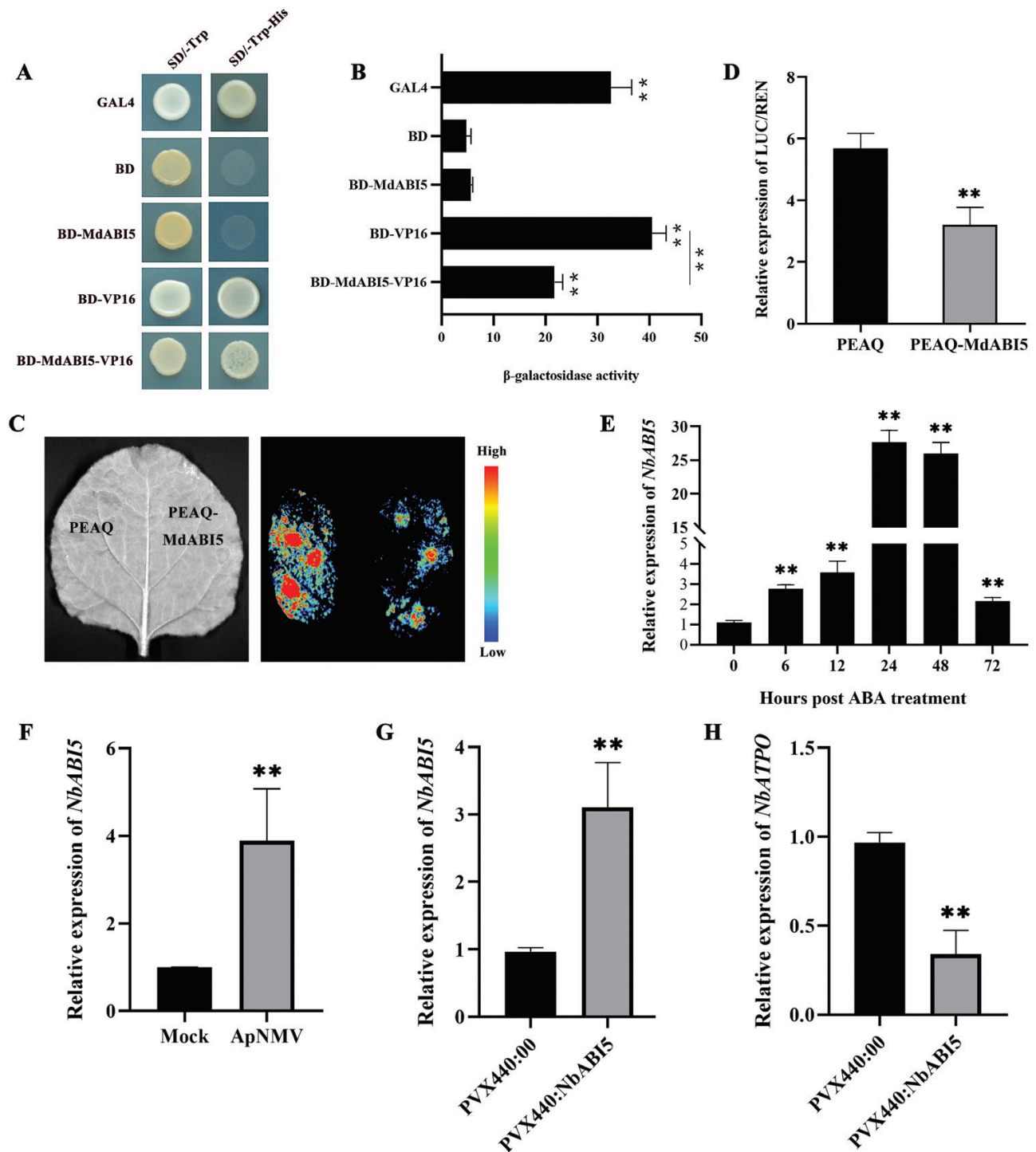
Fig. 6. ABI5 negatively regulates *ATPO* expression. (A) Transactivation activity analysis of *MdABI5* in yeast cells. SD-Trp/-His medium was used to examine transformant growth. At least three yeast colonies were tested for each construct, and representative results are shown. GAL4 and BD-VP16 were used as positive controls; BD was used as negative control. (B) β-galactosidase activity analysis of the yeast colonies grown on SD/-Trp medium in (A). The enzyme activity indicates the transcriptional activity. At least three independent experiments were performed, and three samples were used per experiment. (C) Transient luciferase (LUC) reporter assay of *MdABI5*. PEAQ-MdABI5 was used as effector vector, and then co-infiltrated with the promoter *LUC* gene into *N. benthamiana* leaves. The LUC fluorescence of the agroinfiltrated leaves was measured after 48 h. (D) Quantification of *trans*-activity of *MdABI5* in (C) by LUC/REN assay. (E) Time course analysis of the transcript levels of *NbABI5* in 100 μM ABA-treated plants at 0, 6, 12, 24, 48, and 72 h by RT–qPCR. (F) RT–qPCR analysis indicating *NbABI5* transcript levels up-regulated by ApNMV in *Nicotiana benthamiana* plants at 14 dpi. (G) *NbABI5* was transiently overexpressed in *N. benthamiana* plants, and the transcript levels was determined by RT–qPCR. (H) RT–qPCR analysis showing *NbATPO* transcript levels in *NbABI5*-overexpressed *N. benthamiana* plants. Error bars indicate the SE of the mean (*n*=3). Asterisks indicate significant differences (*, *P*<0.05; **, *P*<0.01), as determined by two-sample unequal variance directional *t*-test. The expression of *NbATPO* and *NbABI5* was determined relative to that of mock-treated plants.

mock plants (Fig. 6G), while the *NbATPO* mRNA levels decreased ~70% in the *NbABI5*-overexpressed plants (Fig. 6H). These results indicated that ABI5 negatively regulates *ATPO* expression.

ABI5 negatively regulates ATPO *by binding to its promoter*

It has been demonstrated that ABI5 binds to the ABRE *cis*-element within the target gene promoter region in Arabidopsis and *N. benthamiana* (Wang *et al.*, 2013; Cui *et al.*, 2021). Here, to verify the binding of MdABI5 to ABRE element, we conducted a yeast one–hybrid (Y1H) assay with the synthesized sequences containing three copies of the ABRE element (ACGTG) and the mutant mABRE (ATTTG) (Fig. 7A). The recombinant plasmids pAbAi–3×ABRE and pAbAi–3×mABRE were independently incorporated into the genome of the Y1H Gold yeast strain. The recombinant plasmid pGADT7-MdABI5 and the empty vector pGADT7 were then independently transformed. All yeast cells grew well on SD/−Leu medium, whereas only yeast cells co-transformed with pGADT7-MdABI5 and pAbAi–3×ABRE grew well on the SD/−Leu medium with 200 ng ml^{-1} aureobasidin A (AbA; Fig. 7B), indicating that MdABI5 can bind to the ABRE element in yeast cells.

To further illustrate how MdABI5 regulates the activity of *MdATPO* promoter, a transient transactivation assay with the GUS expression system was used (Fig. 7C). The tissue-cultured apple leaves co-infiltrated with 35S-MdABI5–eGFP and Pro*MdATPO*-GUS showed shallow GUS staining (Fig. 7D) and the GUS transcript decreased by 50% compared with the control leaves infiltrated with the 35S-eGFP and Pro*MdATPO*-GUS (Fig. 7E). As expected, *N. benthamiana* leaves co-infiltrated with 35S-MdABI5–eGFP and Pro*MdATPO*-GUS showed shallow GUS staining and lower GUS expression than the control (Supplementary Fig. S5).

We further performed a dual-luciferase assay to analyse the regulation of *MdATPO* by MdABI5 in *N. benthamiana* leaves. We first constructed the reporter vector Pro*MdATPO*-LUC and the effector vector 62SKII–MdABI5 (Fig. 7F), and then co-transferred the effector and reporter vectors into *N. benthamiana* leaves. It was found that co-expression of the control vector and the Pro*MdATPO*-LUC produced stronger (*P*<0.05) LUC/REN signals than co-expression of the effector 62SKII–MdABI5 and the Pro*MdATPO*-LUC reporter (Fig. 7G, H). These results line up with the finding that *NbABI5* overexpression decreased *NbATPO* expression (Fig. 6H). Overall, these findings suggest that ABI5 negatively regulates the expression of *ATPO* by directly binding to its promoter.

ABI5 *increases ApNMV infection*

To explore the function of *NbABI5* during ApNMV infection, we performed a VIGS assay to silence the expression of

NbABI5 using the TRV-based VIGS system. A 298 bp PCR fragment representing the partial sequence of *NbABI5* was inserted into the pTRV2 vector to produce TRV:NbABI5. *A. tumefaciens* harbouring TRV1 and TRV:NbABI5 constructs were co-infiltrated into *N. benthamiana* leaves. The empty vector was used as a negative control. RT–qPCR analysis revealed that the expression level of *NbABI5* in silenced plants was only 50% of that in the control plants (Fig. 8A), and expression of *NbATPO* significantly increased (*P*<0.01) about 2.4-fold in *NbABI5*-silenced plants compared with that of mock plants (Fig. 8B). Compared with the TRV vector-inoculated *N. benthamiana* plants, the accumulation level of ApNMV genomic RNA (Fig. 8C, D) and coat protein (Fig. 8E, F) in the *NbABI5* silenced plants was significantly decreased (*P*<0.05). To further transiently overexpress *NbABI5* in *N. benthamiana* plants, the full CDS of *NbABI5* was cloned into the PVX440 vector to generate PVX440:NbABI5 (Fig. 8G), and ApNMV was agro-infiltrated into *NbABI5* transiently overexpressing plants at 5 dpi. The accumulation level of ApNMV genomic RNA (Fig. 8H, I) and coat protein (Fig. 8J, K) in the *NbABI5* overexpressed plants was significantly increased (*P*<0.01) compared with that of empty vector-treated plants. These results indicate that *NbABI5* has a positive effect against ApNMV infection.

Discussion

Plant factors play a critical role in different stages of viral infections. As obligate intracellular organisms, plant viruses must utilize host factors for their invasion, accumulation, cell-to-cell, and long-distance movements (Boevink and Oparka, 2005; Cowan *et al.*, 2018; Venturuzzi *et al.*, 2021). Increasing lines of evidence indicate that ATP synthase subunits in the chloroplast are involved in plant–virus interactions. Tobamoviruses, such as TMV, turnip vein clearing virus, and also potato virus X (PVX) in *N. tabacum* reduced expression level of the messenger RNA of the chloroplast protein ATP synthase-γ subunit (AtpC; Bhat *et al.*, 2013). HC–Pro protein of potato virus Y interacted with the ATP synthase β-subunit in tobacco chloroplasts, leading to a reduced ATP synthase content in both the HC-Pro transgenic and PVY-infected tobacco plants (Tu *et al.*, 2015). ATP synthase α-subunit (ATPsyn-α) was strongly induced in response to infection with an avirulent strain of soybean mosaic virus (SMV), SMV-G5H (Bwalya *et al.*, 2022). In addition, the expression of the biosynthesis genes involved in ABA, salicylic acid (SA), jasmonic acid (JA), and ethylene (ET) increased in response to SMV, when co-inoculated with *ATPsyn-α* (Bwalya *et al.*, 2022), indicating that phytohormones are involved in the ATPsyn-α-mediated defence responses.

Although several studies have reported the association of chloroplast ATP synthase subunits in viral infections, little is known about the mitochondrial ATP synthase subunits that are directly involved in virus–plant interactions. Here, we reported that apple MdATPO physically interacted with ApNMV CP both *in vitro* and *in vivo* (Fig. 2), and the expression of *MdATPO* was
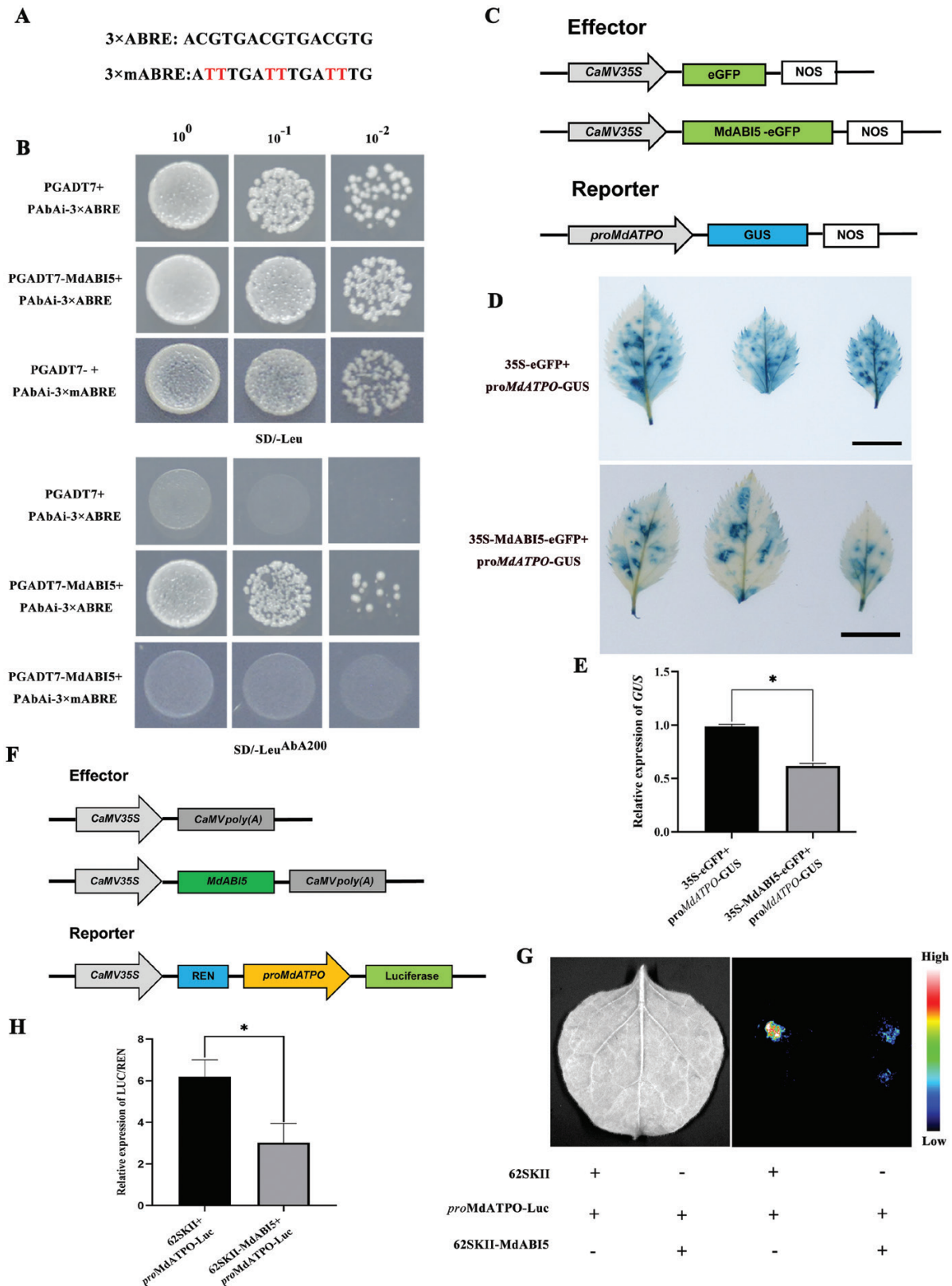
Fig. 7. ABI5 suppresses *ATPO* by binding to its promoter. (A) Sequences of three tandem repeats of ABRE and mABRE elements. (B) Yeast one-hybrid (Y1H) assay to analyse the physical interactions between *MdABI5* and 3×ABRE or 3×mABRE elements. Yeast transformants independently carrying pGADT7-MdABI5 and pGADT7 were diluted 10–100 fold and grown on SD/−Leu (upper panel) and SD/−Leu containing 200 ng ml⁻¹ aureobasidin A

(lower panel), respectively. (C) Schematic diagram of effector and reporter constructs used for GUS expression. Vector contained 35S-MdABI5-eGFP as effector. *MdATPO* promoter fragment (1.86 kb upstream from ATG site) contained ABRE sequence fused with GUS as reporter. (D) GUS staining showing that MdABI5 suppresses *MdATPO* promoter activity in apple leaves. The 35S-MdABI5-eGFP and 35S-eGFP vectors were agroinfiltrated separately along with the Pro*MdATPO*-GUS construct into GL-3 apple leaves, and GUS activity assay was performed at 48 h post-infiltration. Scale bars=1 cm. (E) Quantification of GUS transcript levels in (D) by RT-qPCR. (F) Schematic diagram of effector and reporter constructs used for dual luciferase assay. Vector contained 62SKII-MdABI5 as effector. *MdATPO* promoter fragment (1.86 kb upstream from ATG site) contained ABRE sequence fused with LUC as reporter. (G) The interaction of MdABI5 with the *MdATPO* promoter as shown by a dual luciferase (LUC) reporter system. Pro*MdATPO*-LUC reporter constructs were transiently expressed in *N. benthamiana* leaves along with either control vector 62SKII or 62SKII-MdABI5 effector. LUC signal was imaged at 48 h post-transfection. (H) LUC/REN ratio representing relative activity of *MdABI5* with *MdATPO* promoter in a dual LUC assay shown in (G). Error bars indicate the SE of the mean (*n*=3). Asterisks indicate significant differences (*, *P*<0.05), as determined by two-sample unequal variance directional *t*-test.
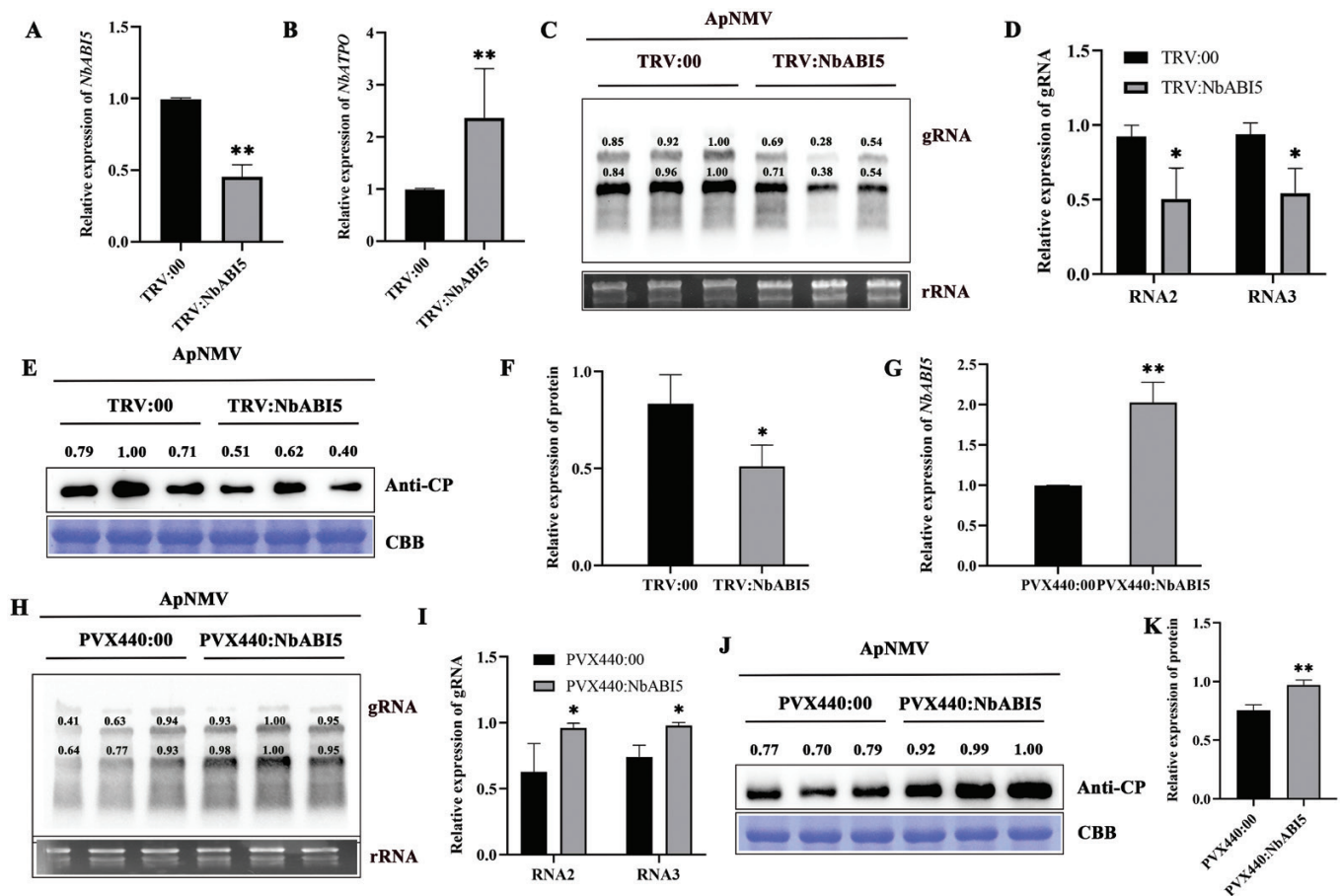
Fig. 8. ABI5 has a positive effect to ApNMV infection. (A) RT–qPCR indicating the silencing of *NbABI5* in *N. benthamiana* plants. (B) RT–qPCR analysis showing *NbATPO* transcript levels in *NbABI5*-silenced *N. benthamiana* plants. (C) Northern blot analysis of ApNMV gENA accumulation in systemic leaves of mock-inoculated and *NbABI5*-silenced *N. benthamiana* plants at 14 dpi. ribosomal RNAs (rRNAs) stained with GelStain served as a loading control. (D) Average values were derived based on the intensity of the bands in (C), and statistical analysis was performed. (E) Western blot results showing the accumulation of ApNMV CP in mock-inoculated and *NbABI5*-silenced *N. benthamiana* plants at 14 dpi. Coomassie Brilliant Blue (CBB)-stained Rubisco large subunit served as a loading control. (F) Average values were derived based on the intensity of the bands in (E), and statistical analysis was performed. (G) *NbABI5* was transiently overexpressed in *N. benthamiana* plants, and the transcript levels were determined by RT–qPCR. (H) Northern blot analysis of ApNMV gRNA accumulation in systemic leaves of inoculated mock and *NbABI5*-overexpressed *N. benthamiana* plants at 14 dpi. (I) Average values were derived based on the intensity of the bands in (H), and statistical analysis was performed. (J) Western blot results showing the accumulation of ApNMV CP in mock-inoculated and *NbABI5*-overexpressed *N. benthamiana* plants at 14 dpi. (K) Average values were derived based on the intensity of the bands in (J), and statistical analysis was performed. The experiments were performed independently three times and representative results are shown. The intensities of bands in western blot analyses were quantified using ImageJ software to compare the virus titre. For (C), (E), (H) and (J), numbers above the blots indicated bands intensities. The expression of *NbATPO* and *NbABI5* was determined relative to that of mock-treated plants. Error bars indicate the SE of the mean (*n*=3). Asterisks indicate significant differences (*, *P*<0.05; **, *P*<0.01), as determined by Student's *t*-test.

down-regulated by ApNMV (Fig. 3). Sequence analysis revealed that MdATPO contained a conserved OSCP domain (Fig. 1A) that is critical for ATP synthase assembly (Müller and Grüber, 2003). The expression pattern analysis showed that *MdATPO* was strongly expressed in mature leaves, which may be related to its role in photosynthetic electron transport during photosynthesis. Previous studies have identified that chloroplast ATP-synthase subunits had negative regulatory effect on virus infection. Silencing AtpC promotes TMV accumulation and pathogenicity in *N. benthamiana* (Bhat *et al.*, 2013). Furthermore, SMV level was reduced in the *ATPsyn-α*-overexpressed soybean and *N. benthamiana* plants (Bwalya *et al.*, 2022). In this study, by using ectopic expression of *MdATPO* in *N. benthamiana* plants, we found that the expression levels of both mRNA and protein of ApNMV significantly decreased in the transgenic lines compared with the empty vector control plants (Fig. 3). In contrast, there was more virus titre in the *NbATPO*-silenced plants (Fig. 3). Therefore, we propose that ATPO acts as a positive regulator, providing resistance in apple and *N. benthamiana* plants to ApNMV infection.

The phytohormone abscisic acid plays critical roles in numerous plant physiological processes including seed germination (Wang *et al.*, 2021), seedling development (Yadukrishnan and Datta, 2021), and leaf senescence (An *et al.*, 2021). Moreover, the prominent contribution of ABA to plant defence response to abiotic stress has long been studied, such as drought (Lim *et al.*, 2022), cold (Wang *et al.*, 2020), and salt stresses (Tao *et al.*, 2011). In response of plants to biotic stress, ABA plays both positive and negative roles, and its effectiveness is dependent on the host–pathogen interaction (Mauch–Mani and Mauch, 2005; Chen *et al.*, 2013). In plant–virus interactions, several studies have demonstrated a positive correlation between ABA levels and antiviral resistance. TMV infection stimulated ABA accumulation (Whenham *et al.*, 1986), and exogenous application of ABA inhibited the accumulation of TMV-cg RNA in systemically infected leaves (Chen *et al.*, 2013), and increased resistance to tobacco necrosis virus (Iriti and Faoro, 2008). Another study, however, has found that ABA negatively regulates plant defence against viruses. Rice black-streaked dwarf virus (RBSDV) infection suppressed ABA biosynthetic genes, and exogenous application of ABA promoted rice susceptibility to RBSDV infection by suppressing the jasmonate pathway, and regulating reactive oxygen species levels (Xie *et al.*, 2018). In this study, we found that the concentration of ABA in ApNMV-infected *N. benthamiana* plants was significantly increased compared with that of non-infected plants. In addition, the expression of three ABA biosynthesis genes, *NbABA1*, *NbABA2*, and *NbNCED1*, were significantly up-regulated under ApNMV infection (Fig. 4). We further investigated the effect of ABA pre-treatment on ApNMV infection. ABA pre-treatment promoted viral accumulation in *N. benthamiana* plants (Fig. 5). Several studies have shown that ABA either up- or down-regulates numerous genes associated with stress responses (Y. C. Huang *et al.*, 2016; Sah *et al.*, 2016; Zhao *et al.*, 2022). Here, we observed that both *MdATPO* and *NbATPO* were down-regulated during ApNMV

infection (Fig. 3), and exogenous application of ABA inhibited the transcription of *NbATPO* (Fig. 5A). These results indicated that ABA negatively modulates plant defence against ApNMV.

Multiple *cis*-elements known as ABA-responsive elements (ABREs) containing an ACGT core motif have been identified in the promoters of ABA-responsive genes (Fujita *et al.*, 2005). As a big transcription factor family, quite a few bZIP transcription factors have been identified to bind to ABREs and regulate the expression of ABA-responsive genes (Sah *et al.*, 2016). Here, we identified nine ABREs in the promoter of *MdATPO* (Fig. 4A; Supplementary Table S3) and four ABREs in the promoter of *NbATPO* (Supplementary Fig. S4; Supplementary Table S4), indicating that *ATPO* is a potential target gene of bZIP transcription factors. Among the studies of the bZIP family, the third sub-family of AREBs (ABA-responsive element binding proteins)/ABFs (ABRE binding factors)/ABI5 (Abscisic acid-insensitive 5) has been extensively studied due to its significant functions in the ABA signalling pathway (Tang *et al.*, 2012). It was demonstrated that ABI5 was involved in the transduction of the ABA signal as well as the response to drought stress (X. Li *et al.*, 2021), salt stress (Zou *et al.*, 2008), and low temperature stress (R. Li *et al.*, 2021). Recently, a study has shown that rice stripe virus (RSV) infection increased the expression of *OsABI5*, a negative regulator of *OsFD1*, resulting in rice susceptibility to RSV (Cui *et al.*, 2021). In this study, we observed that *NbABI5* was up-regulated by application of ABA and ApNMV infection, and NbABI5 negatively regulated *NbATPO* expression (Fig. 6). Further studies revealed that MdABI5 suppressed *MdATPO* promoter activity by binding to ABREs (Fig. 7). These results indicate that ABI5 may has a positive role in plant defence against ApNMV infection. Our subsequent experiments proved that *NbABI5* overexpression enhanced ApNMV infection, whereas *ABI5* silencing had the opposite effect (Fig. 8).

Taking all the results into consideration, we propose a model on the role of the ABI5–ATPO module in the control of ApNMV infection in apple and *N. benthamiana* plants. We have identified that ApNMV infection stimulated ABA accumulation, which represses the transcription of *ATPO* by promoting *ABI5* expression. ABI5 directly binds to the ABREs in the *ATPO* promoter to promote ApNMV infection. Although it has been demonstrated that MdATPO interacts with ApNMV CP, further research is still required to determine how this interaction affects ApNMV infection. Identifying and mutating the critical amino acid residues of MdATPO that allow interaction with ApNMV CP should be the initial step in future research, followed by an evaluation of the effects of blocking this interaction on ApNMV infection.

Supplementary data

The following supplementary data are available at *JXB* online.

Fig. S1. RT–PCR and western blot analysis of *MdATPO* in transgenic *N. benthamiana* plants.

Fig. S2. Morphological phenotypes of empty vector and *MdATPO* overexpression *N. benthamiana* lines 21 d after planting in soil.

Fig. S3. Silencing of *NbATPO* caused stunted phenotype with shortened distance between the leaves of *N. benthamiana* at 14 dpi.

Fig. S4. The predicted *cis*-acting regulatory elements in the promoter sequences of *NbATPO*.

Fig. S5. MdABI5 suppresses *MdATPO* promoter activity in *N. benthamiana* leaves as shown by GUS staining.

Table S1. Primers used in this study.

Table S2. Fragments of *NbATPO* and *NbABI5* used for VIGS.

Table S3. Predicted *cis*-elements of *MdATPO* promoter.

Table S4. Predicted *cis*-elements of *NbATPO* promoter.

Acknowledgements

Author contributions

SL, HW, and CH conceived and designed the research; CH, FX, and JL performed the experiments; ZZ and BZ supervised the research and provided suggestions; CH collected and analysed the data and wrote the manuscript; NH, HW, and SL revised the article. All the authors read and approved the final manuscript.

Conflict of interest

The authors declare that they have no conflicts of interest associated with this work.

Funding

Data availability

The data supporting the findings of this study are available from the corresponding author, Shifang Li, upon request.

References

Amari K, Burgos L, Pallas V, Sanchez-Pina MA. 2007. Prunus necrotic ringspot virus early invasion and its effects on apricot pollen grain performance. Phytopathology **97**, 892–899.

An JP, Zhang XW, Liu YJ, Zhang JC, Wang XF, You CX, Hao YJ. 2021. MdABI5 works with its interaction partners to regulate abscisic acid-mediated leaf senescence in apple. The Plant Journal **105**, 1566–1581.

Aparicio F, Pallás V, Sánchez-Navarro J. 2010. Implication of the C terminus of the Prunus necrotic ringspot virus movement protein in cell-to-cell transport and in its interaction with the coat protein. Journal of General Virology **91**, 1865–1870.

Aparicio F, Vilar M, Perez-Payá E, Pallás V. 2003. The coat protein of prunus necrotic ringspot virus specifically binds to and regulates the conformation of its genomic RNA. Virology **313**, 213–223.

Assunção AG, Herrero E, Lin YF, et al. 2010. *Arabidopsis thaliana* transcription factors bZIP19 and bZIP23 regulate the adaptation to zinc deficiency. Proceedings of the National Academy of Sciences, USA **107**, 10296–10301.

Bhat S, Folimonova SY, Cole AB, Ballard KD, Lei Z, Watson BS, Sumner LW, Nelson RS. 2013. Influence of host chloroplast proteins on Tobacco mosaic virus accumulation and intercellular movement. Plant Physiology **161**, 134–147.

Boevink P, Oparka KJ. 2005. Virus-host interactions during movement processes. Plant Physiology **138**, 1815–1821.

Bwalya J, Alazem M, Kim KH. 2022. Photosynthesis-related genes induce resistance against soybean mosaic virus: evidence for involvement of the RNA silencing pathway. Molecular Plant Pathology **23**, 543–560.

Cantoro R, Crocco CD, Benech-Arnold RL, Rodríguez MV. 2013. *In vitro* binding of *Sorghum bicolor* transcription factors ABI4 and ABI5 to a conserved region of a GA 2-OXIDASE promoter: possible role of this interaction in the expression of seed dormancy. Journal of Experimental Botany **64**, 5721–5735.

Chen L, Zhang L, Li D, Wang F, Yu D. 2013. WRKY8 transcription factor functions in the TMV-cg defense response by mediating both abscisic acid and ethylene signaling in Arabidopsis. Proceedings of the National Academy of Sciences, USA **110**, E1963–E1971.

Cowan GH, Roberts AG, Jones S, Kumar P, Kalyandurg PB, Gil JF, Savenkov EI, Hemsley PA, Torrance L. 2018. Potato mop-top virus co-opts the stress sensor HIPP26 for long-distance movement. Plant Physiology **176**, 2052–2070.

Cui W, Wang S, Han K, Zheng E, Ji M, Chen B, Wang X, Chen J, Yan F. 2021. Ferredoxin 1 is downregulated by the accumulation of abscisic acid in an ABI5-dependent manner to facilitate rice stripe virus infection in *Nicotiana benthamiana* and rice. The Plant Journal **107**, 1183–1197.

Cvetkovska M, Vanlerberghe GC. 2012. Coordination of a mitochondrial superoxide burst during the hypersensitive response to bacterial pathogen in *Nicotiana tabacum*. Plant, Cell and Environment **35**, 1121–1136.

Cvetkovska M, Vanlerberghe GC. 2013. Alternative oxidase impacts the plant response to biotic stress by influencing the mitochondrial generation of reactive oxygen species. Plant, Cell and Environment **36**, 721–732.

Dai H, Li W, Han G, Yang Y, Ma Y, Li H, Zhang Z. 2013. Development of a seedling clone with high regeneration capacity and susceptibility to *Agrobacterium* in apple. Scientia Horticulturae **164**, 202–208.

Dröge-Laser W, Weiste C. 2018. The C/S1 bZIP Network: a regulatory hub orchestrating plant energy homeostasis. Trends in Plant Science **23**, 422–433.

Fujita Y, Fujita M, Satoh R, Maruyama K, Parvez MM, Seki M, Hiratsu K, Ohme-Takagi M, Shinozaki K, Yamaguchi-Shinozaki K. 2005. AREB1 is a transcription activator of novel ABRE-dependent ABA signaling that enhances drought stress tolerance in Arabidopsis. The Plant Cell **17**, 3470–3488.

Hamilton CA, Good AG, Taylor GJ. 2001. Induction of vacuolar ATPase and mitochondrial ATP synthase by aluminum in an aluminum-resistant cultivar of wheat. Plant Physiology **125**, 2068–2077.

He C, Xing F, Zhao X, et al. 2023. The coat protein of the ilarvirus prunus necrotic ringspot virus mediates long-distance movement. Journal of General Virology **104**, 1. doi:10.1099/jgv.0.001829.

Huang S, Van Aken O, Schwarzlander M, Belt K, Millar AH. 2016. The roles of mitochondrial reactive oxygen species in cellular signaling and stress response in plants. Plant Physiology **171**, 1551–1559.

Huang YC, Niu CY, Yang CR, Jinn TL. 2016. The heat stress factor HSFA6b connects ABA signaling and ABA-mediated heat responses. Plant Physiology **172**, 1182–1199.

Iriti M, Faoro F. 2008. Abscisic acid is involved in chitosan-induced resistance to tobacco necrosis virus (TNV). Plant Physiology and Biochemistry **46**, 1106–1111.

Jin D, Wu M, Li B, et al. 2018. The COP9 Signalosome regulates seed germination by facilitating protein degradation of RGL2 and ABI5. PLoS Genetics **14**, e1007237.

Kanai M, Nishimura M, Hayashi M. 2010. A peroxisomal ABC transporter promotes seed germination by inducing pectin degradation under the control of ABI5. The Plant Journal **62**, 936–947.

Kang JY, Choi HI, Im MY, Kim SY. 2002. Arabidopsis basic leucine zipper proteins that mediate stress-responsive abscisic acid signaling. The Plant Cell **14**, 343–357.

Kaur A, Nijhawan A, Yadav M, Khurana JP. 2021. OsbZIP62/OsFD7, a functional ortholog of FLOWERING LOCUS D, regulates floral transition and panicle development in rice. Journal of Experimental Botany **72**, 7826–7845.

Lee SJ, Lee MY, Yi SY, Oh SK, Choi SH, Her NH, Choi D, Min BW, Yang SG, Harn CH. 2002. PPI1: a novel pathogen-induced basic region-leucine zipper (bZIP) transcription factor from pepper. Molecular Plant-Microbe Interactions **15**, 540–548.

Li R, Jiang M, Song Y, Zhang H. 2021. Melatonin alleviates low-temperature stress *via* ABI5-mediated signals during seed germination in rice (*Oryza sativa* L.). Frontiers in Plant Science **12**, 727596.

Li X, Zhong M, Qu L, Yang J, Liu X, Zhao Q, Liu X, Zhao X. 2021. AtMYB32 regulates the ABA response by targeting ABI3, ABI4 and ABI5 and the drought response by targeting CBF4 in *Arabidopsis*. Plant Science **310**, 110983.

Liang J, Wu Z, Zheng J, et al. 2022. The GATA factor HANABA TARANU promotes runner formation by regulating axillary bud initiation and outgrowth in cultivated strawberry. The Plant Journal **110**, 1237–1254.

Lim C, Kang K, Shim Y, Yoo SC, Paek NC. 2022. Inactivating transcription factor OsWRKY5 enhances drought tolerance through abscisic acid signaling pathways. Plant Physiology **188**, 1900–1916.

Liu D, Shi L, Han C, Yu J, Li D, Zhang Y. 2012. Validation of reference genes for gene expression studies in virus-infected *Nicotiana benthamiana* using quantitative real-time PCR. PLoS One **7**, e46451.

Liu S, Wang C, Liu X, Navas-Castillo J, Zang L, Fan Z, Zhu X, Zhou T. 2021. Tomato chlorosis virus-encoded p22 suppresses auxin signalling to promote infection via interference with SKP1-Cullin-F-boxTIR1 complex assembly. Plant, Cell and Environment **44**, 3155–3172.

Liu Y, Schiff M, Marathe R, Dinesh-Kumar SP. 2002. Tobacco Rar1, EDS1 and NPR1/NIM1 like genes are required for N-mediated resistance to tobacco mosaic virus. The Plant Journal **30**, 415–429.

Livak KJ, Schmittgen TD. 2001. Analysis of relative gene expression data using real-time quantitative PCR and the 2(-Delta Delta C(T)) Method. Methods **25**, 402–408.

Logan DC. 2006. The mitochondrial compartment. Journal of Experimental Botany **57**, 1225–1243.

Mauch-Mani B, Mauch F. 2005. The role of abscisic acid in plant-pathogen interactions. Current Opinion in Plant Biology **8**, 409–414.

Møller IM, Rasmusson AG, Van Aken O. 2021. Plant mitochondria - past, present and future. The Plant Journal **108**, 912–959.

Müller V, Grüber G. 2003. ATP synthases: structure, function and evolution of unique energy converters. Cellular and Molecular Life Sciences **60**, 474–494.

Noda H, Yamagishi N, Yaegashi H, Xing F, Xie J, Li S, Zhou T, Ito T, Yoshikawa N. 2017. Apple necrotic mosaic virus, a novel ilarvirus from mosaic-diseased apple trees in Japan and China. Journal of General Plant Pathology **83**, 831–890.

Pallas V, Aparicio F, Herranz MC, Sanchez-Navarro JA, Scott SW. 2013. The molecular biology of ilarviruses. Advances in Virus Research **87**, 139–181.

Roger AJ, Muñoz-Gómez SA, Kamikawa R. 2017. The origin and diversification of mitochondria. Current Biology **27**, R1177–R1192.

Sah SK, Reddy KR, Li J. 2016. Abscisic acid and abiotic stress tolerance in crop plants. Frontiers in Plant Science **7**, 571.

Shi W, Yao R, Sunwu R, Huang K, Liu Z, Li X, Yang Y, Wang J. 2020. Incidence and molecular identification of apple necrotic mosaic virus (ApNMV) in Southwest China. Plants (Basel) **9**, 415.

Smykowski A, Zimmermann P, Zentgraf U. 2010. G-box binding factor1 reduces CATALASE2 expression and regulates the onset of leaf senescence in *Arabidopsis*. Plant Physiology **153**, 1321–1331.

Strathmann A, Kuhlmann M, Heinekamp T, Dröge-Laser W. 2001. BZI-1 specifically heterodimerises with the tobacco bZIP transcription factors BZI-2, BZI-3/TBZF and BZI-4, and is functionally involved in flower development. The Plant Journal **28**, 397–408.

Sun D, Li S, Niu L, Reid MS, Zhang Y, Jiang CZ. 2017. PhOBF1, a petunia ocs element binding factor, plays an important role in antiviral RNA silencing. Journal of Experimental Botany **68**, 915–930.

Sweetlove LJ, Heazlewood JL, Herald V, Holtzapffel R, Day DA, Leaver CJ, Millar AH. 2002. The impact of oxidative stress on *Arabidopsis* mitochondria. The Plant Journal **32**, 891–904.

Tang N, Zhang H, Li X, Xiao J, Xiong L. 2012. Constitutive activation of transcription factor OsbZIP46 improves drought tolerance in rice. Plant Physiology **158**, 1755–1768.

Tao Z, Kou Y, Liu H, Li X, Xiao J, Wang S. 2011. OsWRKY45 alleles play different roles in abscisic acid signaling and salt stress tolerance but similar roles in drought and cold tolerance in rice. Journal of Experimental Botany **62**, 4863–4874.

Tu Y, Jin Y, Ma D, Li H, Zhang Z, Dong J, Wang T. 2015. Interaction between PVY HC-Pro and the NtCF1β-subunit reduces the amount of chloroplast ATP synthase in virus-infected tobacco. Scientific Reports **5**, 15605.

Venturuzzi AL, Rodriguez MC, Conti G, Leone M, Caro MDP, Montecchia JF, Zavallo D, Asurmendi S. 2021. Negative modulation of SA signaling components by the capsid protein of tobacco mosaic virus is required for viral long-distance movement. The Plant Journal **106**, 896–912.

Vlot AC, Laros SM, Bol JF. 2003. Coordinate replication of alfalfa mosaic virus RNAs 1 and 2 involves *cis-* and *trans-*acting functions of the encoded helicase-like and polymerase-like domains. Journal of Virology **77**, 10790–10798.

Wang G, Li X, Ye N, Huang M, Feng L, Li H, Zhang J. 2021. OsTPP1 regulates seed germination through the crosstalk with abscisic acid in rice. New Phytologist **230**, 1925–1939.

Wang H, Blakeslee JJ, Jones ML, Chapin LJ, Dami IE. 2020. Exogenous abscisic acid enhances physiological, metabolic, and transcriptional cold acclimation responses in greenhouse-grown grapevines. Plant Science **293**, 110437.

Wang Y, Li L, Ye T, Lu Y, Chen X, Wu Y. 2013. The inhibitory effect of ABA on floral transition is mediated by ABI5 in *Arabidopsis*. Journal of Experimental Botany **64**, 675–684.

Whenham RJ, Fraser RS, Brown LP, Payne JA. 1986. Tobacco-mosaic-virus-induced increase in abscisic-acid concentration in tobacco leaves: intracellular location in light and dark-green areas, and relationship to symptom development. Planta **168**, 592–598.

Xie K, Li L, Zhang H, et al. 2018. Abscisic acid negatively modulates plant defence against rice black-streaked dwarf virus infection by suppressing the jasmonate pathway and regulating reactive oxygen species levels in rice. Plant, Cell and Environment **41**, 2504–2514.

Xing F, Robe BL, Zhang ZX, Wang HQ, Li SF. 2018. Genomic analysis, sequence diversity, and occurrence of apple necrotic mosaic virus, a novel ilarvirus associated with mosaic disease of apple trees in China. Plant Disease **102**, 1841–1847.

Xiong F, Ren JJ, Yu Q, Wang YY, Lu CC, Kong LJ, Otegui MS, Wang XL. 2019. AtU2AF65b functions in abscisic acid mediated flowering via regulating the precursor messenger RNA splicing of ABI5 and FLC in *Arabidopsis*. New Phytologist **223**, 277–292.

Xu G, Zhong X, Shi Y, et al. 2020. A fungal effector targets a heat shock–dynamin protein complex to modulate mitochondrial dynamics and reduce plant immunity. Science Advances **6**, eabb7719.

Xu Y, Zhao X, Aiwaili P, Mu X, Zhao M, Zhao J, Cheng L, Ma C, Gao J, Hong B. 2020. A zinc finger protein BBX19 interacts with ABF3 to affect drought tolerance negatively in chrysanthemum. The Plant Journal **103**, 1783–1795.

Yadukrishnan P, Datta S. 2021. Light and abscisic acid interplay in early seedling development. New Phytologist **229**, 763–769.

Yu, F, Wu Y, Xie Q. 2015. Precise protein post-translational modifications modulate ABI5 activity. Trends in Plant Science **20**, 569–575.

Yue X, Zhang G, Zhao Z, *et al*. 2019. A cryophyte transcription factor, CbABF1, confers freezing, and drought tolerance in tobacco. Frontiers in Plant Science **10**, 699.

Zhang B, Van Aken O, Thatcher L, *et al*. 2014. The mitochondrial outer membrane AAA ATPase AtOM66 affects cell death and pathogen resistance in *Arabidopsis thaliana*. The Plant Journal **80**, 709–727.

Zhang X, Liu S, Takano T. 2008. Overexpression of a mitochondrial ATP synthase small subunit gene (AtMtATP6) confers tolerance to several abiotic stresses in *Saccharomyces cerevisiae* and *Arabidopsis thaliana*. Biotechnology Letters **30**, 1289–1294.

Zhang Z, Xie YH, Sun P, Zhang FJ, Zheng PF, Wang XF, You CX, Hao YJ. 2022. Nitrate-inducible MdBT2 acts as a restriction factor to limit apple necrotic mosaic virus genome replication in *Malus domestica*. Molecular Plant Pathology **23**, 383–399.

Zhao H, Li Z, Wang Y, *et al*. 2022. Cellulose synthase-like protein OsCSLD4 plays an important role in the response of rice to salt stress by mediating abscisic acid biosynthesis to regulate osmotic stress tolerance. Plant Biotechnology Journal **20**, 468–484.

Zinsmeister J, Lalanne D, Terrasson E, *et al*. 2016. ABI5 is a regulator of seed maturation and longevity in legumes. The Plant Cell **28**, 2735–2754.

Zou M, Guan Y, Ren H, Zhang F, Chen F. 2008. A bZIP transcription factor, OsABI5, is involved in rice fertility and stress tolerance. Plant Molecular Biology **66**, 675–683.